The Desorption Process in MALDI

Klaus Dreisewerd*

Institute of Medical Physics and Biophysics, University of Münster, Robert-Koch-Strasse 31, Münster D-48149, Germany

Received May 28, 2002

Contents

I. Introduction

A matrix-assisted laser desorption ionization (MALDI) "event" constitutes a complex process, involving optical and mechanical phenomena as well as thermodynamic and physicochemical processes of phase transition and ionization. A successful MALDI analysis encompasses several crucial steps: sample preparation, excitation of sample and disintegration of the condensed phase, generation and separation of charges and ionization of analyte molecules, and, finally, extraction, separation according to the mass-to-charge ratio of the ions in the mass spectrometer, and detection.

* E-mail: dreisew@uni-muenster.de. Fax +49-251-8355121. Tel. +49-251-8356726.

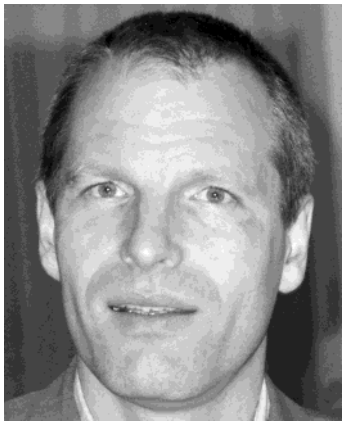

Klaus Dreisewerd was born in Beckum, Germany, in 1961. He received his diploma in Physics from the University of Münster in 1990 and his Ph.D. degree in 1995 under the supervision of Franz Hillenkamp. He moved to the Free University of Amsterdam as a post-doc in the molecular neurobiology department at the end of 1994 and returned to the Münster institute in 1997. His main current interests are in the field of MALDI fundamentals and that of MALDI-MS with pulsed infrared lasers (IR-MALDI).

Despite the rapid acceptance of the method in chemistry and biomedicine after its introduction by Karas and Hillenkamp,[1−4] the underlying mechanisms have been less well understood for a long time and a more comprehensive picture has only recently begun to emerge. Systematic variation of one or more of the relevant "input" parameters is one of the most straightforward experimental tools to obtain insight into the involved mechanisms, and has consequently been utilized in a large number of fundamental studies. The role of the different relevant irradiation (laser) parameters in the desorption/ionization process, as well as those of the matrix and the preparation protocol, have been addressed in these investigations. These included, for example, the role of the laser wavelength, pulse duration, and laser fluence (laser energy per pulse and unit area) for the laser parameters (addressed in section III), and the type of (co-)crystallization and the matter of the incorporation of analyte molecules into matrix crystals for the material side (section IV). In other work, the dynamical parameters of the expanding MALDI particle "plume" have been addressed (section V): the initial kinetic energies and energy distributions of molecules and ions, and the composition of the plume (ion-to-neutral ratio and ejection of particles and clusters versus the emission of molecular constituents). Several researchers have developed theoretical models for the desorption as well as the ionization

10.1021/cr010375i CCC: $44.00
Published on Web 01/24/2003

processes. More recently, large-scale molecular dynamics (MD) simulation studies have added valuable information and helped to close the gap between the experimental results and theoretical considerations.

By far the largest fraction of the experimental investigations has naturally focused on the MALDI ions as detected in a mass spectrometer. When interpreting these data, one has to keep in mind that their generation generally is the result of a convolution of two processes, desorption and ionization, a fact that may easily conceal relevant details of either of the two processes. The employment of supplementary methods, for instance, the recording of the desorbed neutral molecules, can add very valuable information, and several of such experiments have consequently been carried out. These include postionization of neutral molecules, laser-induced fluorescence imaging of the MALDI plume, and trapping plate experiments.

From the different involved aspects, the present article focuses on "desorption". By definition used throughout this article, this will include the excitation of samples, the subsequent phase change, and the dynamics of the material plume expansion.

Primary (matrix) and secondary (analyte) excitation and ionization mechanisms are reviewed in the two closely related articles by Karas and Krüger,[5] and Knochenmuss and Zenobi[6] in this issue.

II. General Overview and Definitions

First reports on the use of pulsed lasers for the desorption/ionization of (neat) organic samples in conjunction with mass spectrometry date back to the 70s.[7−10] CO_2 lasers ($\lambda = 10.6\ \mu$m) and UV lasers emitting in the far-UV with pulse durations in the nanosecond range proved to be most valuable for this "direct" laser desorption/ionization (LDI) from neat samples. In addition to this single-laser LDI approach, resonance enhanced multiphoton-ionization (REMPI; often also noted as resonant ionization mass spectrometry [RIMS]) of neutrally desorbed analyte molecules by a second UV-laser has been and is still widely used.[11] In these cases, desorption is usually accomplished with a pulsed CO_2 laser and molecules are subsequently cooled internally by introducing them into a supersonic molecular beam prior to ionization by, for example, a frequency-doubled dye-laser.

The single laser desorption/ionization approach, for LDI limited to organic molecules of about 1−2 kDa in mass, has received its decisive impetus by the introduction of the two-component MALDI preparation technique, developed in the second half of the 80s.[1−4,12,13] Very generally, analyte compounds are embedded in a surplus of matrix, consisting of small organic molecules, and are co-desorbed upon laser excitation. A useful matrix is believed to provide a number of different essential functions: the first is to isolate analyte molecules by dilution within the preparation, to prevent analyte aggregation. Second, the matrix has to absorb the laser energy via electronic [ultraviolet (UV-) MALDI] or vibrational [infrared (IR-) MALDI] excitation. Third, disintegration of the condensed phase has to take place without excessive destructive heating of the embedded analyte molecules. Last, but not least, an efficient ionization of analyte molecules has to be provided. Other more technical aspects are a sufficient solubility in a suitable (analyte-compatible) solvent and a sufficient vacuum stability.

A large variety of compounds has been empirically tested in the past for their suitability to act as a matrix. Today, analysts commonly make their choice from a relatively small number of established "chemical matrixes", e.g., from benzoic[14] or cinnamic acid[15] derivatives. The actual choice depends on the type of analyte. Some matrix compounds, such as for example, 2,5-dihydroxybenzoic acid (DHB), can, however, be used successfully for a number of quite different applications.

Two closely related techniques have, moreover, been developed. The first is based on the use of suspensions of highly absorbing inorganic "nanoparticles", e.g., cobalt, silicon, or titanium-nitride with diameters in the low nanometer to low micrometer range, in a suitable liquid (typically glycerol). Particle suspension matrixes were first described by Tanaka et al. in 1988.[16] This approach has been taken up again a few times in subsequent years by other groups[17−19] and shown to be useful for the analysis of some compounds that are less compatible with the normal MALDI chemical matrixes, for example, varnishes.[20] In comparison to common MALDI with chemical matrixes, laser desorption from particle suspension matrixes is less soft, however, and accompanied by a higher degree of analyte fragmentation. The method also provides a substantially lower sensitivity.[19] The mass range in which suspension matrixes can be reasonably employed is, therefore, limited to about 10 kDa for peptides/proteins.[19] Other analyte classes have not been investigated in detail. The limitations result essentially from the different way—compared to MALDI with chemical matrixes—of energy deposition and phase transition, mediated by a heated surface. This is believed to result in a too destructive heating of the analyte molecules[19] and an insufficient desorption rate.[21] "Two-phase matrix-",[17] "graphite-assisted-",[20] and "surface-assisted" laser desorption ionization (SALDI[18]) have been introduced as alternative notations for this approach.

Another modification of "surface-MALDI" is the preparation of neat analyte samples on highly porous silicon surfaces. This desorption ionization on silicon (DIOS) technique was introduced by Wei et al. in 1999[22] and has been shown meaningful for molecules in the low (matrix) mass range. The upper mass limit of DIOS is in the low kilodalton range. A so far not satisfactorily resolved problem of the technique is a poor reproducibility from chip to chip. Because of the different mechanisms and their minor analytical relevance, compared to conventional MALDI with chemical matrixes, the surface-MALDI approaches will not be further addressed in the scope of this article.

In by far the most cases, lasers with wavelengths in the near-ultraviolet are today employed for MALDI. Most commonly, either N_2 lasers, emitting

at 337 nm, or frequency-tripled Nd:YAG lasers with a wavelength of 355 nm are used. Pulse durations of these lasers are typically in the range of 0.5 to ~10 ns. Whereas matrix compounds have to exhibit a sufficiently high absorption at the laser wavelength, most analyte compounds will be nonabsorbing in the near-UV. Direct photoexcitation of labile analyte molecules is therefore prevented. A second advantage of the use of the near UV-laser wavelengths is that they induce a relatively low degree of photochemical products such as matrix−analyte adduct formation. These processes have been found to be considerably more prominent if lasers with shorter wavelengths, e.g., 308, 266, and 248 nm (excimer and frequency-quadrupled Nd:YAG lasers), are employed (section III.A). Their successful employment for MALDI has, on the other hand, clearly demonstrated that a certain degree of "direct" absorption by analyte molecules is generally tolerable.

Pulsed infrared (IR) lasers have been found to constitute alternative desorption/ionization laser sources with certain advantages and disadvantages if compared to the more common UV-MALDI mode.[23−26] In the IR, energy deposition is achieved via absorption by vibrational modes of the matrix molecules. Typically, either O−H or N−H stretch vibrations of the molecules are excited at wavelengths around 3 μm. Pulsed erbium solid-state lasers (Er:YAG, $\lambda = 2.94\ \mu$m, or Er:YSGG, $\lambda = 2.79\ \mu$m) with pulse durations between 50 and 100 ns or wavelength-tunable optical parametric oscillator (OPO) laser systems with pulse durations of 5−10 ns are commonly used for IR-MALDI. The applicability of pulsed CO_2 lasers with emission wavelengths around 10 μm has moreover been demonstrated.[27,28] In this case, O−H bending and C−H stretch vibrations of the molecules are excited. A free-electron laser (FEL) with a picosecond pulse substructure has, finally, been employed in a number of studies with essentially fundamental background.[29,30] A unique feature of the FEL is that besides to the 3 μm range, it can also be tuned to the wavelength range of C=O stretch vibrations between 5.5 and 6.5 μm.[29]

Some ambiguity exists in the pertinent literature concerning the terminology used to describe laser-induced material removal. Although MALDI is mostly referred to as a desorption process, "desorption" would, by any more rigorous thermodynamic definition, be reserved to a purely thermal process in which the transfer of individual molecules from the condensed to the gas phase occurs from the outermost layers of the sample. In this sense, desorption is simply the reverse reaction of adsorption. "Sublimation" is somewhat less strictly defined but is usually also seen as transfer of individual molecules. "Vaporization" would include "evaporation" from the outer surface layers as well as (heterogeneous) "boiling", which involves the formation of gas bubbles inside a molten sample volume. "Explosive boiling", also termed "phase explosion", can occur if the material is superheated "beyond" its spinodal and always results in the explosive ejection of entire volume elements.[31−34] Laser ablation or laser ejection are mostly used as nonspecific notation in the latter cases. Material can furthermore be transferred into the gas phase by laser-induced processes of nonthermal nature, e.g., by photomechanical stress[35] or photochemically by direct bond-breaking caused by the absorption of high-energetic photons.[36] Despite the mechanistic differences, "desorption", as commonly used in the MALDI field, "ejection", and "ablation" will be used in parallel throughout this paper.

The article reviews in its first results part (section III) the investigations performed on the role of the relevant irradiation/laser parameters for the desorption process, in particular their effect on the yield of analyte and matrix ions and molecules. The second part (section IV) describes the work performed on the analyte−matrix interaction in the sample. Part three (section V), finally, reviews the investigations carried out on the dynamics of the expanding particle plume. The review focuses on the UV-MALDI case. A similar overview by the author of the characteristics of IR-MALDI will be published separately.[24]

III. Irradiation Parameters

Table 1 lists the MALDI-relevant irradiation (laser) parameters. The range as usable in principle for MALDI on the most common axial-TOF instruments is indicated in the second column; the third column denotes values as typical for a laser spot size of 100 μm in diameter. The extended range in column two results essentially from a strong effect of the laser spot size on some of the values. The applicable fluence range would also extend to higher values if high-pressure[37] instead of vacuum MALDI sources were employed.

A. Laser Wavelength and Matrix Absorption

The significance of a sufficient optical absorption of the matrix at the laser wavelength was already recognized in the early days of MALDI.[1,15,38] As a rule of thumb, spectrum quality generally increases with absorption,[39] although, once the absorption exceeds a certain value, differences tend to level out.[40] Spectral absorption profiles of solid matrix preparations can differ considerably from solution spectra:[39−43] absorption profiles of the solid-state tend to be broadened, in particular toward longer wavelengths, resulting in a red-shift of the peak absorption. Figure 1, reproduced from the article by Horneffer et al.,[39] demonstrates this for the example of four dihydroxybenzoic acid positional isomers.

A detailed investigation of the wavelength dependence in the typical MALDI wavelength range between 248 and 355 nm is, somewhat surprisingly, still pending. Employing four discrete laser wavelengths of 266, 308, 337, and 355 nm, Horneffer et al. found that the matrix-quality of the four dihydroxybenzoic acid derivatives of Figure 1 depends distinctly on the employed wavelength/molar absorption.[39] Qualitatively, the best mass spectrometric performance was obtained at wavelengths near the absorption maximum. Allwood et al. reported similar results for a series of matrix compounds in a comparative study with wavelengths of 337 and 308

Table 1. Definition of the Relevant MALDI Irradiation (laser) Parameters, Range of Values Meaningful for UV-MALDI, and Typical Values for Common (axial-TOF) MALDI Conditions at a Laser Spot Size of ~100 μm in Diameter

parameter	range	typical values for common matrixes and a laser spot diameter of ~100 μm
laser wavelength, λ	193−430 nm	(266), 337, 355 nm
laser penetration depth into the sample, δ (= α^{-1}; α: absorption coefficient)	~ 50−300 nm	50−200 nm
photon energy at laser wavelength, E_ν	2.9 eV (430 nm) − 6.5 eV (193 nm)	4.71 eV (266 nm), 3.72 eV (337 nm), 3.53 eV (355 nm)
laser pulse duration, τ	0.5 − ~20 ns, (560 fs [a])	0.5−10 ns
diameter of laser spot on sample surface	1 μm − ~1 mm	50−200 μm
energy per single laser pulse as applied to the sample, E	10 nJ − 10 μJ [b]	1−10 μJ
mean power of a single laser pulse, averaged over the pulse duration ($1/e^2$-definition)[c], P_{avg}	1−5 × 10^3 W [b]	10^2 W − 5 × 10^3 W
fluence (energy per laser pulse and unit area), H [d]	30 − ~10,000 Jm^{-2} [b]	30−600 Jm^{-2}
irradiance (fluence divided by the laser pulse duration), I	3 × 10^5 − 1 × 10^9 Wcm^{-2} [b]	1 × 10^6 − 5 × 10^7 Wcm^{-2}

[a] Ref 53. [b] Values strongly depend on the focal laser spot size. [c] For near Gaussian pulse shape the peak power is about two times the average power. [d] Often denoted as F or Φ, instead.

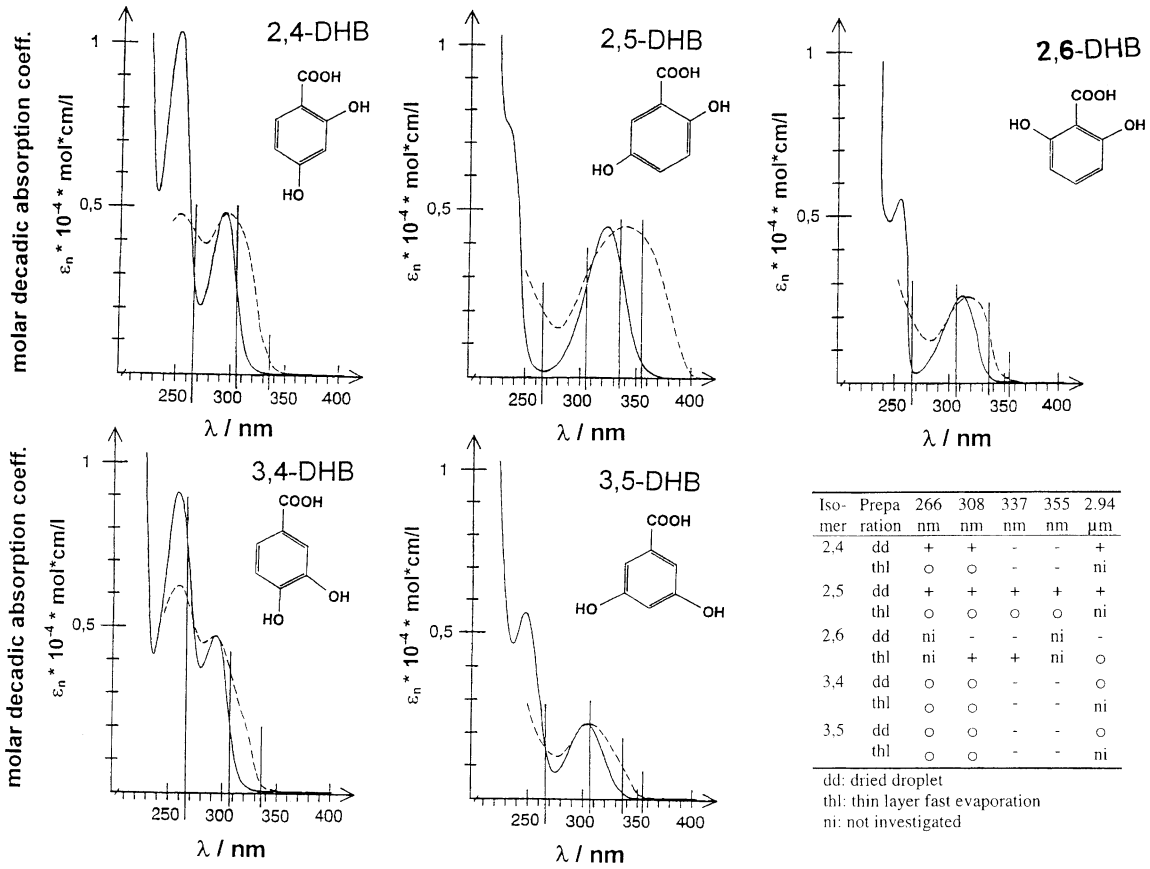

Iso-mer	Prepa ration	266 nm	308 nm	337 nm	355 nm	2.94 µm
2,4	dd	+	+	-	-	+
	thl	○	○	-	-	ni
2,5	dd	+	+	+	+	+
	thl	○	○	○	○	ni
2,6	dd	ni	-	-	ni	-
	thl	ni	+	+	ni	○
3,4	dd	○	○	-	-	○
	thl	○	○	-	-	ni
3,5	dd	○	○	-	-	○
	thl	○	○	-	-	ni

dd: dried droplet
thl: thin layer fast evaporation
ni: not investigated

Figure 1. UV-absorption spectra of five positional isomers of dihydroxybenzoic acid. Solid lines: spectra obtained from a water/ethanol solution (9:1, v/v); dashed lines: diffuse reflection spectra of solid powder dispersed in $BaSO_4$. For the solution spectra, the values for the molar decadic absorption coefficients are absolute. For the diffuse reflection spectra $\log(1/R)$ is plotted (R: reflectivity), normalized to the value of the absorption coefficient in solution at the long wavelength maximum. The table summarizes the mass spectrometric quality of cytochrome *C* ion signal detection when desorbed from the different DHB positional isomer matrixes and at the four UV-wavelengths of 266, 308, 337, and 355 nm. The right column shows data for IR-MALDI, acquired with a 2.94 μm-Er:YAG laser, for comparison. +: good protein signals; ○: weak protein signals; −: no protein signals. (Courtesy of V. Horneffer; reproduced with permission from ref 39; copyright Elsevier Science, 1999).

nm.[44] The two investigations demonstrate that it can be worthwhile to test matrixes of potential interest at alternative wavelengths. In line with earlier observations made by Beavis and Chait,[45] Horneffer et al. also found that the extent of photochemical reactions between matrix and analyte is usually

enhanced with photon energy. This was in both studies observed as an enhanced matrix−analyte adduct formation.

A consequence of the broadened solid phase absorption profiles is that matrixes can be employed for MALDI-MS analysis at laser wavelengths surprisingly outside their solution absorption bands. The absorption profile of 3-hydroxypicolinic acid (3-HPA) matrix in solution, for example, peaks at about the XeCl excimer wavelength of 308 nm and is almost at baseline at 355 nm.[46] However, a nearly indistinguishable performance of this matrix, widely used for the analysis of oligonucleotides, is found at 266, 308, 337, and 355 nm, as was first noted by Wu et al.[46] (the N_2 laser wavelength of 337 nm was not employed in the study of Wu et al. but is today most widely used). Surprisingly, this matrix even exhibits a higher threshold fluence for ion detection at 308 than at 337 nm.[47]

Chen et al. employed a frequency-doubled Ti-sapphire laser system to study the wavelength region of 360−450 nm,[40] normally not utilized for MALDI. In this study, MALDI spectra were recorded up to a wavelength of about 430 nm for some common cinnamic acid derivatives. The authors noted that mass spectra were barely affected by the photon energy over a wide wavelength range. Only when the long wavelength side of the absorption band was approached, some changes in the distribution of multiply charged ions became apparent. Chen et al. adopted solid-state absorption coefficients from measurements of Allwood et al.[42] to calculate the deposited energy per volume at threshold fluences in their experiments. They determined this value to be about 8 kJ cm^{-3} for near-surface volume elements (∼10 nm depth), and found it to be essentially constant over the wavelength range in which MALDI spectra could be generated, which means that over a wide wavelength range a lower absorption coefficient is simply compensated by a higher (threshold) fluence. Chen et al. noticed, however, that if the absorption approached some critically low value, analyte ions could not be produced anymore, regardless of how high a laser fluence was then applied. Remarkably, matrix ions were, however, still found to be generated at these long wavelengths. It should be noted that the value of 8 kJ cm^{-3} as determined by Chen et al. for the energy per volume at the ion threshold is somewhat higher than those reported in most other studies (most researchers report values closer to 1 kJ cm^{-3}), possibly because of an indirect method of determining the laser spot size used in the study by Chen et al.

Other groups have tried to extend the useful wavelength range toward the visible by employing new classes of chemical matrixes with larger conjugated electron systems.[48−52] Such matrixes can potentially allow the employment of high-power pulsed diode lasers, which are not available for the UV, and, hence, miniaturization of the instruments. Compared to the established UV-MALDI matrix/wavelength systems, these attempts have so far, however, brought about only very limited success.

B. Threshold Fluence, Laser Beam Profile, and Size of Irradiated Area

There is quite a large variation in the values reported in the literature for the threshold fluence at which the onset of ion generation has been detected, and, hence, also for the energy densities in the excitation volume. In the first MALDI experiments with the LAMMA 1000 instrument, a threshold irradiance of $\sim 5 \times 10^7$ W cm^{-2} was, for instance, reported by Karas et al. for a nicotinic acid matrix and a laser wavelength of 266 nm.[1,3] Given the 10 ns pulse duration of the Nd:YAG laser used in that study, this corresponds to a fluence as high as 5000 J m^{-2}. Succeeding studies by Beavis and Chait, in which a comparable frequency-quadrupled Nd:YAG laser was employed, already reported considerably lower irradiance values on the order of 1×10^6 W cm^{-2}, corresponding to a fluence of about 100 J m^{-2}.[45] Most of the more recent work, in which threshold MALDI fluences were explicitly addressed, are in line with these lower irradiance values, e.g., refs 53−56 and 66.

The differences in the determined threshold values apparently originate from a surprisingly strong influence that the size of the irradiated area (focal beam size) has on the MALDI threshold fluence.[55,56] Karas et al., in fact, operated their microprobe instrument with a laser spot size between 3 and 30 μm, whereas in modern MALDI instruments spot sizes between 50 and 200 μm in diameter are commonly realized. It is important to note that the recorded dependence cannot simply be accounted for by a reduction of the ion signal in linear proportion to the varied irradiated area. The generally very steep increase of ion intensities with laser fluence (section III.C) would much more rapidly compensate for a decrease in laser spot size, i.e., the reduction in area from which ejection can occur.

Investigations in which the size of the irradiated area has been systematically varied were reported by Ingendoh et al.[55] and Dreisewerd et al.[56] Both studies revealed an increase in threshold fluence by about 1 order of magnitude when going from the largest test spot size of 280 and 200 μm in diameter, respectively, to the smallest one of 10 μm in diameter (in both studies). The results on the threshold fluence−spot size dependence from the work by Ingendoh et al. are reprinted in Figure 2.

An experimental difference in the two investigations was that a Gaussian beam profile in the focal plane was used in the study by Ingendoh et al. (in that case the diameter was defined by the usual $1/e^2$-intensity definition), whereas a "flat-top" profile was realized in the second work by means of a fiber optic assembly. The relative similarity in the outcome of the two studies shows that the exact beam profile is apparently not of prime importance for the spot-size dependence, probably at least not as long as these are reasonably smooth.

The study of Dreisewerd et al. has also addressed the desorption of neutral (matrix) molecules, detected by postionization. Their ejection was found to show a similar, albeit slightly less strong dependence on laser spot size than that of the "direct" ions.

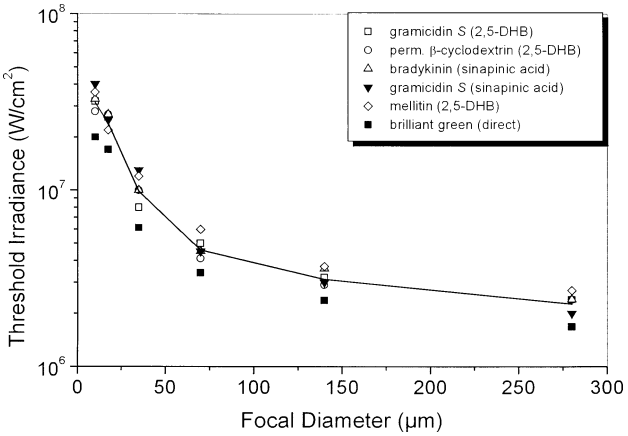

Figure 2. Plot of threshold irradiance versus focal diameter for MALDI-MS of different test compounds and matrixes as indicated in the figure legend; matrixes are denoted in parentheses; the dye brilliant green was desorbed directly, i.e., without matrix, from a small film on the sample target. The beam profile of the employed N_2 laser ($\lambda = 337$ nm, $\tau = 3$ ns) had a (spatial) Gaussian intensity shape. Focal diameters are according to the $1/e^2$ beam waist definition. The solid line represents multiple data set interpolation. (Courtesy of A. Ingendoh; reproduced with permission from ref 55; copyright Elsevier Science, 1993).

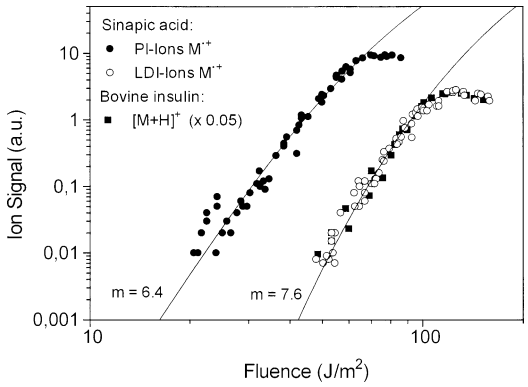

Figure 3. Signal intensities of directly desorbed ions and postionized molecules as a function of desorption laser fluence. (●) Photoionized (PI) sinapinic acid matrix molecules $M^{\bullet+}$, (○) directly desorbed (LDI) molecular ions $M^{\bullet+}$ of sinapinic acid, (■) MALDI ions $(M+H)^+$ of bovine insulin, 5734 Da. An N_2 laser with a flat-top beam profile of 200 μm diameter was employed for desorption ionization. Postionization was achieved with a 248 nm KrF-excimer laser pulse of ~20 ns pulse duration, delayed with respect to the desorption laser pulse by ~1 μs. The postionization laser beam was aligned for broad overlap with the MALDI plume. Each data point represents a single desorption event. Signal intensities were evaluated by peak integration. Insulin ion signal intensities have been scaled to the matrix ion signals for better comparison. The solid lines are fits to a quasi-thermal desorption model. The numbers next to the data indicate the power m as it would be derived from a simple power law fit to the data. (Reproduced with permission from ref 56; copyright Elsevier Science, 1994).

The reasons for the strong spot-size dependence have not been elucidated so far. A likely one is a change in the ratio between molecular desorption and that of clusters,[57] with an increase in cluster generation for small spot sizes, but more detailed work on this aspect is clearly pending. The decrease of laser spot size to diameters on the order of a few to 10 micrometers is furthermore likely accompanied by a sizable change in plume expansion characteristics (section V.B). Such a change is also indicated by the observation made by Ingendoh et al. of a decreased mass resolution (larger ion signal width) at small laser spot sizes.[55]

Under carefully controlled irradiation conditions, matrix and analyte ions were found to exhibit essentially the same threshold fluence[55,56,66] (Figure 3, reproduced from ref 56). To some extent, the exact values of analyte and matrix threshold depend on the analyte-to-matrix (A/M) ratio in the sample,[58] however. For high analyte concentrations, fluence thresholds are sometimes even found to be lower for analyte than for matrix ions, which means that for fluences close to the threshold matrix ion signals can be entirely absent in the spectrum. Knochenmuss et al. have coined the term "matrix-suppression effect" to describe this peculiar observation.[59,60] They suggest that matrix ions are "quenched" by effective charge-transfer reactions within the dense analyte−matrix plume.

Zhigilei and Garrison have extended the concept of the two regimes, desorption of individual molecules at low, and ablation of a mixture of individual molecules and clusters above a distinct fluence threshold in several papers.[57,61−64] These researchers have, moreover, suggested that this transition threshold may in fact correspond to the MALDI ion threshold. In terms of the signal intensity−laser fluence curves, a precipitous drop in signal intensities should, therefore, be expected at the ablation threshold. Such a "physical MALDI threshold" has also been discussed before in other experimental[65] and theoretical work.[82]

Recent experimental work by Westmacott et al., however, indicates that a sharp desorption/ionization threshold is rather unlikely to exist under well-defined MALDI conditions.[66] A single-ion counting, time-to-digital conversion (TDC) detection scheme was used in this work, allowing a very sensitive detection of ions as well as rapid summation over a large number of desorption events. A flat-top beam profile was, moreover, used in this study to optimize irradiation conditions. Westmacott et al. have in parallel recorded the "normal" analogue threshold with a digital storage oscilloscope. Using the TDC detector, the fluence range in which analyte (and matrix) ions were recorded could be extended by a factor of about three toward lower values (Figure 4). It is worth noting that the definition of the "threshold" was somewhat disparate for the two methods used in the study of Westmacott et al. As in the previous investigations with analogue detection schemes,[56,74] this threshold was defined as the fluence at which 50% of individual exposures yielded a clearly discernible ion signal of, e.g., $S/N > 2-3$. The threshold in the TDC measurements was on the other hand determined by summation over a few hundred to a few thousand single exposures.

The fluence range covered by the single ion counting measurements corresponds to a range in the number of intact ions generated (and detected) on average per laser pulse of about 4 orders of magnitude (Figure 4). The number of insulin ions produced

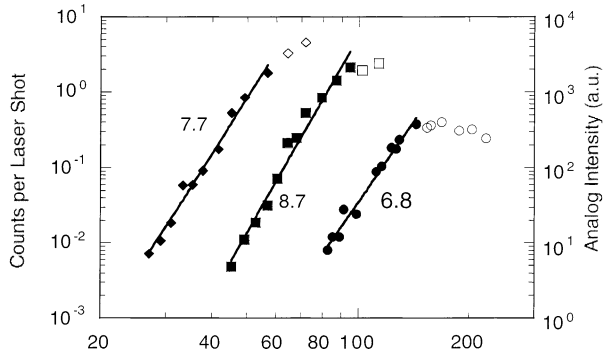

Figure 4. Measured signal intensities of molecular ions of bovine insulin desorbed from a sinapinic acid matrix as a function of laser fluence. An axial-time-of-flight (TOF) mass spectrometer was used and desorption/ionization was achieved with an N_2 laser ($\lambda = 337$ nm, $\tau = 3$ ns). The circles represent analogue measurements with a digital oscilloscope and individual single laser shot desorption ionization events, the squares pulse-counting TDC measurements with an active detector (MCP) area of 1 mm in diameter, and the diamonds pulse-counting measurement with an active detector area of 20 mm in diameter. Between a few hundred to several thousand single shot mass spectra have been accumulated in the TDC measurements. Open symbols represent the onset of detector saturation (Reproduced with permission from ref 66; copyright Elsevier Science, 2002).

at the analogue ion threshold was estimated by Westmacott et al. to be on the order of 20−100, which, in other words, implies that at the low fluence side of the TDC measurements less than one (intact) ion is on average generated per laser pulse. In the low fluence range, the probability for the generation of a specific ion was, therefore, measured in the TDC experiments rather than the actual number. Despite this fundamental difference, the dependence of ion intensity on laser fluence was found to be essentially identical in the low and high fluence ranges (Figure 4).

Preliminary experiments, in extension of the above work, have indicated that the probing of the very low fluence range is experimentally not restricted to the use of a TDC detection scheme. By employing a sensitive analogue detector and summation over a similar high number of events as in the TDC experiments, a similar decrease in accessible fluence range was indeed observed.

C. Increase of Ion Signals with Laser Fluence

Above the ion threshold, MALDI signal intensities generally increase steeply with laser fluence (Figures 3 and 4).[53,54,56,66−71] At fluences exceeding the useful MALDI range, which for axial-TOF instruments typically extends from threshold to fluences about 2−3 times above, extensive fragmentation and other side effects are found to first saturate the increase of the intact ion signal, and, if the fluence is further elevated, even to reverse it. Analyte and matrix ions essentially behave in the same manner[56,66] (Figure 3), independent of the molecular weight of the embedded analyte compounds.[56] The "saturation" of the ion intensity curves at high laser fluences is likely to result from side effects such as fragmentation reactions and detector saturation.

To find a suitable measure for the increase of ion signal intensity Y with fluence H, the experimental curves are for convenience frequently fit by power functions of the form $Y \sim H^m$.[65,68,74] It should be noted that a physical meaning underlying this equation, for example, in terms of a multiphoton process of the order m, can be ruled out. Values for m between 5 and 10 have been determined this way for MALDI from typical laser spot sizes of 50−200 μm in diameter. The slope has been found to depend on the matrix[56,66,68] and to some extent on the instrumental configuration.[66] In particular, the laser spot size was found to influence m considerably.[56] Desorption from very small laser spots below ca. 50 μm in diameter results in a much more shallow increase of molecular ion intensities with fluence.

The fluence dependence of the desorption of neutral (matrix) molecules was addressed in postionization experiments with a second laser by Spengler et al.,[68] Mowry and Johnston,[72,73] Dreisewerd et al.,[56,74] and Schürenberg et al.[75] Like for the "direct" MALDI ions, postionization signal intensities also increase steeply with desorption laser fluence (Figure 3), albeit with a slightly lower slope m. The higher values for the direct ions are likely to reflect an additional fluence dependence of the ionization process. Compared to the other studies, Mowry and Johnston reported a lower slope m of 1−3, only, for the postionization signals, and of 2−4 for the direct ions.[72] The reason for this discrepancy is not known.

In all of the above studies, desorption of neutral molecules was found to set in at fluences considerably below the threshold for the detection of direct ions, by about a factor of 2−3.[56,68,74] The results show that at the common analogue ion threshold a high to very high amount of neutral molecules is set free, and, moreover, that the detected ions will in general only comprise a very small fraction of the overall desorption plume.

Applying Beer's law (and neglecting reflection losses at the surface), the energy per volume deposited into the sample by the laser can straightforwardly be calculated to

$$\frac{dE(z)}{dV} = \alpha H_0 e^{-\alpha z} \qquad (1)$$

provided the solid-state absorption coefficient α at the excitation wavelength is known. H_0 is the fluence at the surface ($z = 0$), and z is the depth in the material. For volume elements at the surface ($z \cong 0$) the equation simplifies to

$$\frac{E}{V} = \alpha H_0 \qquad (2)$$

Because of the low photon fluxes at typical MALDI laser fluences, nonlinear absorption can be ruled out to be of major importance for the overall energy deposition. Using (semi-) quantitative absorption coefficient values for matrix preparations,[39,42] energy densities in near-surface volumes (~10 nm) on the order of several ten to about hundred kJ mol^{-1} are determined at the MALDI threshold,[56] if common laser spot sizes of 50−200 μm in diameter are

applied. These values are close to the combined heats of fusion and vaporization of the matrix materials. Overall, the phase transition from the solid to the gas phase will, therefore, inevitably have a predominant thermal component.

D. Laser Pulse Duration

Lasers with pulse durations between ca. 0.5 and 10 ns are typically employed for UV-MALDI-MS. The less frequently used excimer lasers expand this range to ~25 ns. Longer laser pulses are believed to result in a destructive thermal excitation of analyte molecules before a disintegration of the sample and the release of molecules into the gas phase can take place.[76] A sufficiently fast excitation is, therefore, regarded as one of the key prerequisites for a successful MALDI analysis. Upon laser heating, competing processes take place, among which are fragmentation reactions and desorption. The functionality of MALDI suggests that the characteristic decay rates at the achieved temperatures are lower than those for the desorption/ablation channel.

Frequently, a differentiation is made between fast fragmentation channels ("in-source-decay", ISD[77]) with time constants on the order of the phase transition process and a slower "post-source" unimolecular decay (PSD[78,79]) with time constants on the order of or even above the flight-times in a TOF instrument. The extent of the metastable decay and the decay rates depend strongly on the type of the analyte (e.g., peptides versus oligonucleotides) and the matrix. Matrix compounds are therefore sometimes classified as "hot" (e.g., alpha-cyano-3-hydroxybenzoic acid [αCHCA]), inducing a high degree of metastable analyte fragmentation, and "cold" (e.g., 2,5-DHB), leading to a softer desorption/ionization of labile analytes. The reasons for the differences are not finally clarified. They are likely to lie either in the physicochemical properties of the matrixes, resulting in a different energy transfer during the ionization step, or in dissimilar plume dynamic properties, resulting in different extents of energetic collisions or collisional cooling.

Vertes et al. have discussed that "subliming" matrixes with a low "sublimation temperature" will generally promote the desorption of intact analyte molecules. These authors have also conducted calculations on the heat transfer between the excited host (matrix) and embedded guest (analyte) molecules.[76,80] Besides for the need for sufficiently short laser pulses, they noted the necessity of a sufficient dilution of analyte molecules in the matrix. A too high analyte concentration was calculated to lead to an enhanced transfer of energy from the matrix lattice vibrations to the intramolecular vibrational modes of the embedded analyte molecules and consequently to their thermal degradation. Vertes et al. concluded that for adequately diluted analyte/matrix preparations, it is essentially the frequency mismatch between lattice phonons and intermolecular vibrations that provides for a sufficiently delayed equilibration among all inter- and intramolecular degrees of freedom ("bottleneck model"): matrix and analyte molecules co-desorb before this equilibrium is attained. Similar considerations on the frequency mismatch between lattice and molecular vibrations of molecular solids have been made by Dlott.[81]

With respect to potential pulse duration effects, two energy dissipation pathways have to be particularly considered: heat transport and energy dissipation by stress waves. For nanosecond laser pulse durations, desorption essentially takes place in the regime of thermal confinement, i.e., laser pulse durations are shorter or at most about the time constants for heat transport, τ_{th}. In a one-dimensional picture, justified by the large aspect ratio between laser spot size diameter and laser penetration depth into the sample, τ_{th} can be approximated by

$$\tau_{th} = \frac{\rho c_p}{4\lambda_{th}}\delta^2 \qquad (3)$$

where δ is the laser penetration depth, ρ is the density of the material, c_p is the specific heat, and λ_{th} is the thermal conductivity. The factor of 1/4 accounts for the geometry of the excited volume, a shallow cylinder: the lateral dimension across the laser focus of ~100 μm exceeds that of the laser penetration depth of ~100 nm by 3 orders of magnitude. Using values for 2,5-DHB of $\rho = 1.57 \times 10^3$ kg m^{-3}, $c_p = 1.045 \times 10^3$ J kg^{-1} K^{-1}, and $\delta = 110$ nm according to the solution absorption spectrum,[39] and further approximating λ_{th}, unknown for 2,5-DHB, by that of water ice of 0.5 W m^{-1} K^{-1}, a value τ_{th} of ~10 ns is calculated for this matrix. This value is on the order of typical laser pulse durations, and a relatively homogeneous temperature distribution within the excited volume must, hence, be expected. Lasers with longer pulse durations are consequently to be expected to be accompanied by substantial heat conduction "losses" out of the excited volume during the laser pulse. More detailed experimental studies on this aspect are still pending, mainly due to the lack of appropriate laser sources with pulse durations in the interesting time region.

Photomechanical processes have first been discussed by Johnson to be potentially relevant for the MALDI case.[82] The build-up of stress in the sample would become a significant factor in the overall process if laser pulse durations were shorter or on the order of the characteristic transport time τ_{ac} for the propagation of a (photoacoustic) stress wave through the excitation volume. τ_{ac} is generally approximated by

$$\tau_{ac} = \delta {v_s}^{-1} \qquad (4)$$

where v_s is the speed of sound in the material. Estimating v_s to 2000−3000 ms^{-1} and δ to 50−200 nm, τ_{ac} follows as 17−50 ps. With typical laser pulse durations in the nanosecond range, photoacoustic stress is therefore unlikely to contribute significantly to the overall process. Stress confinement can however be expected to become relevant if short pulses in the lower or subpicosecond range are employed (see below).

Material ablation induced by strong tensile stress (spallation) is regarded as an effective low energy-

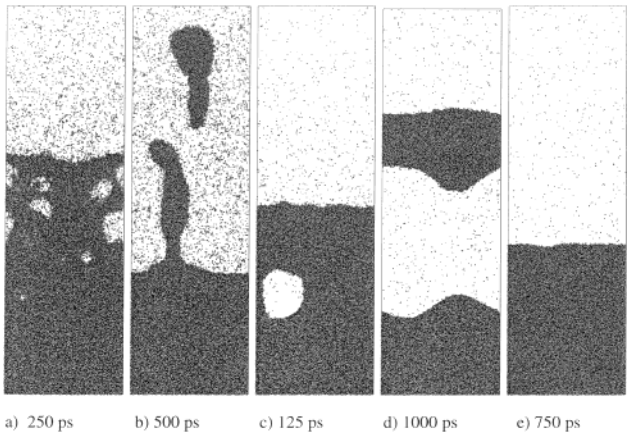

Figure 5. Snapshots from MD computer simulations in the desorption and ablation regime, recorded at different times after ceasing of the excitation pulse (indicated below the snapshots). Each dot represents one matrix molecule with properties according to the breathing sphere model. Temporally rectangular excitation pulses of 150 ps (a,b,e) and 15 ps (c,d) in duration, respectively, have been simulated, corresponding to thermal and stress confinement conditions. Fluences are 40 J/m^2 (a,b) and 31 J/m^2 (c,d), which is in both cases close to the ablation threshold of 35 J/m^2 for the thermal and 29 J/m^2 for the stress confinement regime. The "laser" penetration depth was set to 50 nm. The part of the computational cell shown in the figure is a 40 × 130 nm window; the bottom of the window corresponds to 40 nm below the original surface level, the top corresponds to 90 nm above the level of the original surface. Snapshot (e) shows the case of excitation at a lower fluence in the desorption regime. In the desorption regime only monomeric molecules but no clusters are emitted. Snapshots taken in this fluence regime are indistinguishable for thermal and stress confinement conditions. (Courtesy of L. V. Zhigilei, University of Virginia, 2002).

density pathway in various laser applications apart from MALDI, for instance, in laser ablation of (low absorbing) tissue.[83] Ablation by spallation has, moreover, been discussed as a possible pathway for IR-MALDI where optical absorption coefficients are generally lower than in the UV by 1−2 orders of magnitude.[57,84] However, more recent investigations on the pulse duration effect in IR-MALDI raise substantial doubt on the validity of these considerations and render spallation rather unlikely as an important pathway for most IR-MALDI laser−material combinations.[85]

Next to the rapidly dissipating photoacoustic stress, the build up of notable "hydrodynamic" pressure will occur if a large number of collisional interacting molecules are desorbed (like in MALDI) to form an (initially) dense "gas phase", and can act as driving force for a rapid plume expansion. These gas-phase dynamics are discussed in more detail in section V.B.

Molecular dynamics simulations by Zhigilei and Garrison on the microscopic picture of laser desorption/ablation with and without (photomechanical) stress confinement, simulated by excitation with 150 ps (assumed thermal confinement only) and 15-ps-long pulses (thermal and stress confinement) have recently also indicated relevant mechanistic differences in the two confinement regimes.[57,61] Figure 5 shows five snapshots from the MD calculations for the thermal (Figure 5a,b) and stress confinement regimes (Figure 5c,d). Comparable laser fluences slightly above the "ablation threshold" have been used in both cases. The additional photomechanical component in the regime of stress confinement was found to reduce the threshold fluence by a factor of about 1.2 for the model matrix compound. The numbers below the figures indicate the (snapshot) time after ceasing of the excitation pulse. Each sphere in the figure represents an individual matrix molecule. At 125 ps, the formation of a void is clearly visible for the 15 ps long stress confinement excitation case (Figure 5c). This void grows further with time and finally results in the disrupture and ejection of a bulk volume (Figure 5d). Note that, in contrast to heterogeneous boiling, the void formation does not go along with a sizable density of gas-phase molecules inside the encased volume nor with a diffusion toward the surface. Formation of such voids is not detected in the thermal confinement regime (Figure 5a,b). Here, a foamlike intermediate phase is observed instead, from which individual molecules and single droplets emerge (Figure 5b). Figure 5e, finally, represents the low-fluence desorption regime in which solely individual molecules are released. Snapshots in this fluence range yield an identical picture for both confinement regimes.

In the recent past, the MD work of Zhigilei and Garrison has come considerably closer to represent "true UV-MALDI conditions", which is in particular due to the extension of the simulated excitation times from 15 to 150 ps (15 ps were used in the foregoing work of the authors[61,86,87]) and spatial simulation volumes, which are now covering typical UV-laser penetration depths on the order of 50−100 nm.[57] As a consequence, very intriguing pictures of the process have been presented in recent work of these authors.[57,88,92]

Unfortunately, the previous simulation results for the 15-ps-long excitation pulses, entailing stress confinement, are frequently still adopted by others to resemble UV-MALDI conditions, although this is apparently incorrect. It also appears that some of the inherent limitations and necessary simplifications that all MD simulations naturally have to cope with and their consequences for a correlation with "real world" conditions are sometimes not fully recognized. Some of the limitations are, in fact, likely to have a notable, if not strong effect on the outcome. A number of simplifying assumptions on the physicochemical material parameters and boundary conditions have to be introduced into the computational setup simply to get the simulations running on a reasonable temporal and spatial scale and with acceptable computing time. In the "breathing sphere model" approximation of Garrison and Zhigilei, particles are, therefore, represented by simple spheres with one "internal" degree of freedom only. Other simplifications are the setup of the "matrix" as a noncrystalline "amorphous solid"[89] and the use of temporarily rectangular excitation pulses.

The maximum dimensions of the computational cells which are realistically calculable are nevertheless about a few tens to about one hundred nanometers in lateral (i.e., in the plane of the surface)

direction only, and, hence, still several orders of magnitude below experimental laser spot sizes. In axial, i.e., in the direction of the surface normal, about one micrometer is accessible. Although this is sufficient to correctly simulate the laser penetration depth, gas phase dynamic processes in the expanding plume can only be simulated to a very limited extent. With respect to the duration of the excitation pulses, Zhigilei et al. argue that the 150 ps case, i.e., that of thermal confinement, should also represent common UV-MALDI conditions with lasers emitting with pulse durations in the low nanosecond range.[57] It is however not fully evident why a difference by about 1 order of magnitude should not result in at least some further changes, for instance, caused by further reduction of the residual photoacoustic pressure[57] and an enhanced equilibration of temperatures in the sample.

Zhigilei and Garrison have addressed several of these aspects in recent developments, for instance, by the adjustment of boundary conditions,[90] the employment of bicomponent systems,[91] by using a bead-and-spring model to approximate a three-dimensional molecular analyte structure,[92] and by introducing a combined MD (phase transition)−Monte Carlo (gas-phase dynamics) simulation.[93,94] These latest approaches are likely to further close the gap between the theoretical and the experimental world soon.

Experimental investigations on the role of the laser pulse duration in UV-MALDI have been reported by Demirev et al.[53] and Dreisewerd et al.[74] In the latter study, two nitrogen lasers with pulse durations of 0.55 and 3 ns were compared. Neither mass spectrometric results nor the threshold fluences were found to be notably affected by changing the laser pulse duration in this test range. The results also demonstrate that for about nanosecond long excitation pulses two-photon processes apparently do not play a major role in the overall MALDI process.

Demirev et al. employed a nitrogen laser (337 nm) with a pulse duration of 3 ns, on one hand, and the frequency-doubled output of a mode-locked dye laser generating 560-fs-long pulses of 248 nm wavelength on the other. The dye laser was also used without frequency doubling at 496 nm wavelength. Although a direct comparison of pulse duration effects is in this study somewhat hampered by the difference in the laser wavelengths, several interesting features can be deduced: First, a reduced quality of the mass spectra and an enhanced analyte fragmentation was notable for the 560 fs pulse excitation. Although, following the above considerations, a substantial change in desorption mechanisms has to be expected for the ultrashort pulse duration, the enhanced analyte fragmentation is unlikely to be a direct result of this transition since ablation under stress confinement conditions should lead to internally cooler rather than hotter analyte molecules.[57] The increased fragmentation of analyte ions can instead straightforwardly be explained by extensive photodissociation of analyte molecules by nonlinear processes. In fact, as a result of nonlinear excitation of matrix molecules, mass spectra of bovine insulin were generated from a ferulic acid matrix at 496 nm, although ferulic acid is transparent at this wavelength. Previous non-MALDI comparison studies with pico- and femtosecond versus nanosecond lasers on neat organic samples, reported by Antonov et al.,[95] Karas et al.,[1] and Chekalin et al.,[96] revealed a similar trend toward enhanced molecular fragmentation.

Second, Demirev et al. noted about equal threshold fluences for the two laser pulse durations, in agreement with the outcome of the MD simulations. A factor of 1.2 as predicted by the MD work would clearly be within the experimental accuracy of that study. A notably reduced increase of signal intensities of the intact molecular ions with fluence as observed in the study by Demirev et al. for the 560 fs laser pulse can again be accounted for by enhanced photofragmentation.

Short 30-ps-long laser pulses of 355 nm wavelength from a frequency-tripled Nd:YAG laser have been employed in a study by Knochenmuss and Vertes.[97] This work focused on the generation of 2,5-DHB matrix ions; results for analyte ions were not reported. Knochenmuss and Vertes noted a remarkable effect on matrix ion generation when the sample was irradiated by two splitted pulses from the same 30 ps laser. Both pulses were delayed relative to each other by means of an optical delay line and the energy of the individual pulses was kept below ion threshold. Two maxima in the ion intensity−delay time dependence were observed: the first maximum was expectedly observed at zero delay when both pulses hit the sample coincidentally, and was followed by a rapid drop with delay time down to a minimum ion intensity at a delay time of ∼0.5 ns. Increasing the delay further, however, was found to raise the ion intensity again until a second maximum at a delay time of about 2 ns was reached. For longer delay times, the DHB signal intensities were found to decrease approximately exponentially with a characteristic time constant on the order of a few nanoseconds. In a succeeding article, Knochenmuss interpreted these results in terms of competing rate-dominated processes of ionization and de-excitation of excited molecules and accounted the second maximum by the foregoing onset of phase transition and expansion, initiated by the first pulse.[98] He assumed the preceding disintegration to reduce the intermolecular loss processes within the solid, with a consequently enhanced overall ionization efficiency. The results of the work by Knochenmuss and Vertes also indicate the storage of electronic excitation energy in the MALDI solid or selvedge for a time frame of a few nanoseconds.

E. Fluorescence Studies

On the basis of the results of previous studies by Ehring and Sundqvist, who recorded the fluorescence decay times of laser excited matrix samples[99] also to be on the order of a few nanoseconds, Knochenmuss and Vertes discussed whether S_1 singlet states possibly serve for the energy storage. More recent investigations by Lüdemann et al., employing an improved experimental setup with higher temporal resolution, revealed that the singlet state lifetimes

Table 2. Singlet Life Times τ_S of Typical MALDI Matrixes[a]

matrix	τ_S/ns	λ/nm
ferulic acid	0.2	450
3-hydroxypicolinic acid (3-HPA)	0.4	420
2,5-dihydroxybenzoic acid (2,5-DHB)	0.6	420
3,4,5-trimethoxycinnamic acid	0.7	425
2-aminobenzoic acid	20	425

[a] λ is the fluorescence emission wavelength used to determine the singlet lifetime. Microcrystalline matrix samples were irradiated with 337 nm from a nitrogen flash lamp emitting pulses of ca. 4−5 ns duration (fwhm). (Courtesy of H.-C. Lüdemann[265]).

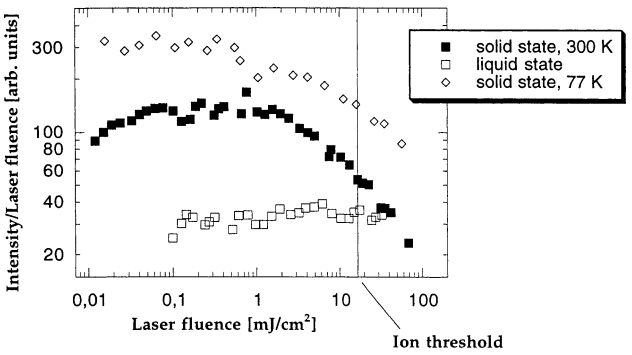

Figure 6. Luminescence intensity/laser irradiance ratio (fluorescence yield) of photoexcited 2,5-DHB sample as a function of the laser irradiance, state of aggregation, and sample temperature. Excitation laser wavelength, 355 nm; pulse width, ~6 ns. The liquid-state preparation contained 10^{-2} mol L^{-1} 2,5-DHB in ethanol−water (1:1, v/v). Luminescence intensity is the wavelength and time-integrated fluorescence intensity as recorded with a grating spectrograph and an optical multichannel analyzer. (Courtesy of H. Ehring; reproduced with permission from ref 99; copyright John Wiley & Sons, Ltd., 1995).

of most typical matrixes in the solid state are more likely to be subnanosecond than above, however (Table 2).[100] A significant contribution of phosphorescence, which would be indicative of long-lived triplet states, was not detected in either of the two luminescence studies. Knochenmuss stressed that once in the gas-phase S_1 lifetimes of the molecules and, hence, fluorescence decay times can become sizably longer and then be on the order of a few tens of nanoseconds.[98]

Ehring and Sundqvist and Lüdemann et al. have also determined the fluorescence yield. Significant quenching of the fluorescence due to annihilation (likely S_1-S_1 state annihilation) was observed in both studies even for fluences considerably below the MALDI threshold. Figure 6 shows the results from the work by Ehring and Sundqvist for differently prepared 2,5-DHB matrix samples. The quenching is indicated by the lower than proportional increase of the fluorescence with fluence. Lüdemann et al. suggested that singlet−singlet state annihilation gives rise to one molecule in a higher excited singlet state and one molecule in the ground state, and, furthermore, that the pooling of the energy of two excited singlet states at one site in the crystal may give rise to the formation of primary matrix ions in UV-MALDI. They also presented a numerical model to fit the data with rate equations for the excitation and annihilation processes. The authors emphasized that the assumption of S_1-S_1 state annihilation gave excellent fit results to their experimental laser induced fluorescence (LIF) data (a 355 nm Nd:YAG laser was employed in this set of experiments), whereas a modeled resonant two-photon excitation (as a second potentially effective process) only led to very poor fits.

F. Phase Transition Models

Models put forward in the literature for the UV-MALDI desorption process range from thermal desorption of individual molecules, surface layer-by-layer sublimation/evaporation[76,80,82] to volume ablation by phase explosion[57,101,102] and volume ablation caused by laser-induced pressure pulses.[82] Laser ablation by heterogeneous ("normal") boiling, involving an (intermediate) liquid phase and generation of (large) vapor bubbles and their diffusion to the surface has recently been found to be a probable process for IR-MALDI from glycerol and long excitation laser pulses of ~100 ns in duration[24] (the laser penetration depth of glycerol at the Er:YAG laser 2.94 μm excitation wavelength is ~1.5−2 μm), but appears unlikely for most solid-state UV-MALDI matrixes.[103] Mixed processes have, finally, also been discussed.[57] Often the term "collective process" is used to describe the MALDI mechanisms, which is particularly justified for those cases that involve volume ablation, but also in the scope of the below discussed gas-phase dynamics of the plume expansion (section V.B).

The preceding paragraphs have elucidated that the actual pathways of phase transition depend substantially on the laser and material properties. Therefore, an overall complex rather than a uniform MALDI picture must be expected if all usable laser/material combinations shall be included. The succeeding sections will further confirm this complexity. The, in the recent past, widely discussed phase explosion model, involving "superheating" of the excited sample volume to a thermodynamically metastable state and eventual spinodal decomposition,[103,104] does therefore not appear likely to hold for MALDI in general.

Phase explosion occurs if the rate of laser energy deposition into the sample exceeds that of the consumption by melting and evaporation or sublimation, and other (solid state) energy dissipation pathways. The material is driven to a metastable superheated state. In case of a liquid and in the absence of nucleation sites, it can remain metastable and be further heated until the spinodal temperature is reached. Further heating beyond this thermodynamic limit will lead to instantaneous spinodal decomposition. The critical temperature at which spinodal decomposition sets in strongly depends on the pressure. Sudden tensile stress, as for example produced by the reflection of laser-induced photoacoustic stress waves at the solid (liquid)−vacuum interface, can lead to a sudden decrease in the spinodal temperature and initiate the phase explosion process. Indications for such a mechanism have recently indeed been observed in short-pulsed OPO IR-laser (τ = 6 ns) excitation of glycerol.[24] Due to the larger laser penetration depth, IR-MALDI is generally accompanied by substantially higher photoacoustic stress

than UV-MALDI, however. A unique feature of spinodal decomposition (in contrast to heterogeneous "normal" boiling) is that it leads to a very rapid (homogeneous) generation of microcavities on a large spatial scale.[105] As a result, ablation encompasses the entire unstable (liquid) volume. The assessment of phase explosion as a relevant process for UV-MALDI is somewhat complicated by the fact that inhomogeneous molecular microcrystals are prepared in almost all cases, whereas most experimental and theoretical work on spinodal decomposition has been performed either on liquids or well-defined solid-state systems such as metals, semiconductors, polymers, or ceramics.

The question whether (some) solid state matrixes may undergo melting as an intermediate phase instead of direct sublimation or disintegration by fracture has hardly been addressed. Microscopic pictures of irradiated large matrix crystals and the observation of structured surface corrugations suggest that melting and recondensation may indeed occur for some compounds (e.g., sinapinic acid[106]), although micrographs of other matrixes are not really unequivocal (Figure 9, section IV). Finally, the rapid phase transition is also accompanied by a drastic change in entropy of the system, which can further drive the decomposition.

From the experimental studies, the ones performed on the influence of the laser fluence appear especially informative since all models will include this parameter in form of the deposited energy. In evaporation/sublimation-like processes, the rate of ejected molecules will generally be determined by an exponential Arrhenius dependence on sample temperature. Von Allmen pointed out that for short-pulsed (nanoseconds and below) laser excitation and a thermal vaporization process, the yield of ejected molecules can be set proportional to the rate at the peak sample temperature in good approximation.[107] In case of a thermal process, the yield can, in a general form, hence, be described by:

$$Y \sim P \exp\left(\frac{-E_a}{k_B(T_0 + BH)}\right) \qquad (5)$$

where Y is the yield (number) of ejected molecules, E_a is the activation energy of the process, T_0 is the initial sample temperature, and k_B is Boltzmann's constant. H is the laser fluence, and B is a conversion factor describing the transformation of laser pulse energy into (lattice) temperature of the sample. To first order, B can be approximated by $(1 - R)\alpha(\beta c\rho)^{-1}$, where R accounts for reflection losses at the surface and β accounts for other processes not leading to a temperature increase (e.g., fluorescence); α is the absorption coefficient, c is the specific heat, and ρ is the density. P is a preexponential factor that will in general include a (less strong) additional temperature dependence (and entropy effects).

As was pointed out by Vertes et al.[76] and Dlott,[81] equilibrium over all degrees of freedom will in general not be achieved on a low nanosecond time scale and an energy flux into matrix lattice vibrations may preferentially take place.[81] $T_0 + BH$ as defining the lattice temperature may, therefore, temporarily be higher than in thermal equilibrium. Neglecting the latter, a laser fluence on the order of 100 J m^{-2} as typical for the MALDI threshold can straightforwardly be calculated to lead to a temperature increase on the order of a few to several hundred Kelvin.

Dreisewerd et al. have applied eq 5 to fit their experimental data on the yield of postionized (matrix) molecules (Figure 3).[56] Activation energies, E_a, on the order of 0.6−0.8 eV were determined for desorption in this work, in good agreement with values determined in rapid heating studies on comparable organic compounds.[108] Dreisewerd et al. showed that the direct MALDI ion data can be reasonably fitted as well by the same equation if a higher E_a value of about 1.3−1.8 eV is applied. Despite the good quality of the fit, with respect to the underlying mechanisms it must be assumed that the ion yield as the common mass spectrometric measure will in general not be described correctly by eq 5, since it does not, for example, include the dependence of molecular excitation and ionization on fluence, as well as any secondary ionization reactions.[6,109] Extended fit procedures applied by the authors but not included in the original article[56] revealed that similarly good fits are indeed obtained if a prefactor proportional to H or H^2 is included in the equation to account for photoexcitation of molecules. In this case, a reduced E_a of about two times the value for desorption of neutral matrix molecules was found to best fit the experimental data.

Zhigilei et al. have argued that the mere reference to postionized neutral molecules as well as monomeric ions will neglect the possibly significant fraction of material ablated in form of clusters (Figure 5), and can, therefore, give a misleading picture.[57] Indeed, a striking finding of their MD work is that although, according to the simulations, the overall yield of ejected material exhibits a sharp increase at the ablation threshold, the yield of monomeric molecules, and presumably ions, continues to follow the Arrhenius-like dependence on fluence. No sharp increase in the yield of monomeric plume constituents were therefore discernible at the ablation threshold, which can possibly explain why such a threshold has so far not been detected in any of the experimental MALDI studies.[56,66] Below the ablation threshold, Zhigilei et al. found molecular ejection to be well described by an Arrhenius dependence (eq 5). Above the threshold, the overall material ejection was, however, found to be best fitted by a volume photoablation (phase explosion) model of the form:

$$Y \sim \delta \ln^n\left(\frac{H}{\delta(E_v^* - cT_0)}\right) \qquad (6)$$

where δ is the laser penetration depth, E_v^* is a critical energy density, and c is the specific heat of the material; n equals one for a flat-top and two for a Gaussian beam profile. Note that the equation is only meaningful for fluences $H > H_{cr} = \delta(E_v^* - cT_0)$. In this model, material is removed down to a sample depth at which the deposited energy per volume

equals a critical energy density, the cohesive energy of the material. Assuming a thermally activated process (in contrast to, e.g., photochemical bond breaking for high photon energy processes), photoablation would be essentially equivalent to the above phase explosion model. It should be added that photoablation also constitutes the acknowledged model for a variety of laser material processing applications, ranging from the removal of tissue[34,110] and polymers[111] to that of metals.[112] A clear experimental proof (or disproof) of its applicability to UV-MALDI is, however, still pending.

Recording of the overall material ejection as a function of laser fluence, preferentially with direct comparison to the ion yield, would be a nice way to differentiate directly between the proposed mechanisms. Also the above-discussed ablation threshold may be detected this way, if present. Unfortunately, due to the very low amounts of material ejected per laser pulse in UV-MALDI, such measurements are anything but straightforward to realize.

In one such attempt, Qvist et al. have utilized a quartz microbalance to measure the rate of material ejection from a ferulic acid matrix, either directly from the matrix-covered quartz balance surface, or indirectly by using the balance as a collector device.[67] Both modes were, unfortunately, found to be connected with large measurement errors, caused by, e.g., the thermal "background evaporation" of ferulic acid, damping of the quartz oscillations due to the macroscopic preparations themselves, in particular in case of laser desorption from the balance surface, and unknown sticking coefficients and re-evaporation in case of the collection mode. Decisive answers are, therefore, difficult to draw from these results. In light of improved preparation protocols for the production of very homogeneous thin matrix layers the microbalance approach seems very worthwhile to reconsider, however. Moreover, several new matrixes with lower vapor pressure than ferulic acid have been described in the recent past.

An alternative approach to measure the overall material ejection rate has been described recently for IR-MALDI measurements.[24] In this case, a piezoelectric sensor was used to record the material ejection-related recoil momentum. Samples were prepared directly on the metallized piezo ceramic surface. With an at least 1−2 orders of magnitude higher amount of material ejected in IR-MALDI, a successful adaptation of this photoacoustic detection principle to UV-MALDI is, however, very demanding. Preliminary experiments carried out in the author's laboratory show that further improvements on the experimental setup are indeed necessary to achieve the needed sensitivity.

Vertes et al.[113] and Knochenmuss[98] have set up a set of rate equations to "calculate" the phase transition and "hydrodynamics" of the expanding plume. Both works provide distinct predictions on some of the experimental quantities, such as the achieved temperatures, number of desorbed particles, and temporal and spatial number density in the expansion plume and their dependence on, for example, the laser fluence. Knochenmuss has extended the previous work by Vertes et al. and has also included excitation and relaxation rates for S_1 and S_n states, e.g., fluorescence decay, as well as energy pooling and primary matrix ionization reactions. He found the calculated fluorescence yield as a function of laser fluence to be in excellent agreement to experimental data by Lüdemann et al.[100] if certain assumptions on the rates of the above mechanisms were made.

G. Backside Illumination Geometry

An experimental approach to differentiate between different, possibly superimposing contributions to the overall MALDI process, in particular between thermal, photochemical and photomechanical pathways, is the employment of "backside" irradiation of samples. In fact, the LAMMA 500 instrument (Leybold Heraeus, Köln, Germany), one of the first commercial laser mass spectrometers, utilized this irradiation geometry.[114] In the LAMMA 500, samples are in general prepared on SEM grids, covered by a Formvar film support. The laser hits the sample from behind. Because of the small laser focal size and high fluences used in this instrument, samples are often "perforated" and ejection processes identical to the top-illumination case may therefore dominate the outcome. The concept of backside illumination, often, somewhat incorrectly, also called "transmission geometry" has also been adopted in more recent work, e.g., to provide for a technically flexible laser beam delivery.[115,116] Schürenberg et al., moreover, employed it for a thermalization of the plume, as a predecessor to more recent high-pressure MALDI sources.[117]

Fundamental experiments performed by Lindner,[118] Ehring et al.,[119] and Golovlev et al.[120] have been carefully designed to avoid any direct photoexcitation of matrix crystals. Ehring et al. used a 200-nm-thick, opaque gold foil for laser pulse absorption and energy deposition. Samples were prepared on the front surface of the foil and an N_2 laser ($\tau = 3$ ns) used for backside excitation. Lindner employed gold and copper foils of a few micrometers thickness as substrates and compared them to normal LAMMA 500 preparations on Formvar-coated grids; he utilized a Nd:YAG laser ($\lambda = 266$ nm, $\tau = 10$ ns) for energy deposition. Finally, Golovlev used a 0.75-mm-thick layer of mercury, encased between sapphire substrates, to block the fundamental 1.06 μm output of a Nd:YAG laser ($\tau = 7$ ns) and to generate a rapid photoacoustic pulse of similar width. This stress wave was, after propagation through the sapphire and the samples, prepared on the sapphire, found to be sufficient to lead to ejection of charged particles. The authors called this process laser-induced acoustic desorption (LIAD). The detection of analyte ions as large as insulin and cytochrome *C* from a picolinic acid MALDI matrix was reported in this work. Golovlev et al. found this matrix to be particularly useful because it formed exceptionally smooth "glassy" films, which was apparently a prerequisite for a sufficient acoustic coupling. The type of ions, observed in their backside illumination experiments, e.g., in terms of protonation or cationization, was not discussed by the authors.

However, Ehring et al. noted significant differences in the ion patterns of matrix and some analyte

compounds if mass spectra generated by back- and frontside irradiation were compared. In case of the tested gramicidin *S*/2,5-DHB system, backside irradiation led to the exclusive generation of cationized analyte molecules, whereas top-illumination produced both protonated and cationized gramicidin *S*. Significant differences were moreover found for the matrix ions: protonated but no radical 2,5-DHB matrix ions were detected in backside illumination, whereas the radical ion species is always observed along with the protonated matrix and with comparable signal intensities when 2,5-DHB samples are irradiated in top-illumination mode. Ehring et al. discussed these differences within the scope of photochemical pathways of matrix ionization and their general relevance for MALDI. In contrast to Golovlev et al., Ehring et al. related the ejection of molecules in backside irradiation geometry to a thermal process, induced by heat conduction from the heated foil. Although a particular thin gold foil was indeed used by Ehring et al., in view of the other work, at least a combined thermal-photoacoustic mechanism seems more likely to account for their results.

Lindner, finally, resumed his early work[121] on the subject and reported a considerable dependence of the mass spectrometric outcome on the type of analyte. He discussed these differences with respect to the acoustic desorption of presumably "preformed" and non-preformed ions.[118] The three investigations elucidate that photoacoustic stress waves can disrupt MALDI matrixes and release imbedded or attached analyte molecules. Moreover, the disrupture apparently provides for the generation of charges sufficient for analyte ionization. A greater importance for normal MALDI is yet not likely since essentially thermal processes must clearly be assumed to dominate the overall phase transition in the conventional top-side illumination case.

H. Ejection of Clusters

Whereas phase transition by surface sublimation/evaporation would predominantly lead to the ejection of individual molecules and relatively small, probably short-lived clusters, bulk volume ablation by phase explosion was more likely to go along with the expulsion of large clusters or even chunks of material. The identification and characterization of clusters in the MALDI plume could, therefore, serve as a tool to differentiate between different mechanisms. Regardless of the details of the phase transition, besides for very low desorption rates, the particle density in the material cloud will in the very first stage resemble almost that of the solid state. With an expansion speed on the order of several hundred ms^{-1} (section V.A), this density will drop steadily but remain sizable for several hundred nanoseconds if not microseconds, depending of course strongly on the laser fluence. Very little is known about the time scale on which analyte molecules and ions lose their "matrix shell" during this expansion.[122] Time-resolved spectroscopic measurements on the plume development might be a means to provide some answers. In the context of MALDI, such measurements have not yet been performed, however.

In fact, MALDI mass spectra as acquired on axial-TOF instruments always exhibit a high level of background "noise" on which the discernible matrix and analyte signals reside. This background, often referred to as "chemical noise",[123] consists of unresolved ions, almost evenly spread over the entire *m*/*z* scale. These chemical noise ions are likely to stem from the decay of clusters as well as from pure molecular decay in the acceleration region of the ion source. Simple signal integration reveals that from the overall number of charges generated per desorption event these unresolved background ions even make out the largest fraction.[124] Although the presence of "chemical noise" in axial-TOF MALDI mass spectra is widely recognized, and actually forms the major reason for the practical MALDI sensitivity limit, its nature has hardly been addressed. Only, Krutchinsky and Chait have recently reported investigations on its origin, in this case, however, carried out with an ion trap detector preceded by an intermediate-pressure collisional damping interface for ion transfer, which may easily yield deviating results if compared to the normal vacuum sources of axial-TOF instruments.[123] Under these experimental conditions, chemical noise signals could be identified to essentially originate from the decay of matrix clusters of different size. 2,5-DHB was investigated in this work.

In this context, an only scarcely discussed aspect is whether analyte compounds may be incorporated into organic (matrix) crystals while preserving part of their water of hydration.[125] These hydration shells, if present, were likely to significantly change the bonding between matrix and analyte molecules and, therefore, also to change the cluster decay dynamics. Under conventional MALDI conditions, complex biomolecules are interestingly enough, however, almost never detected with any preserved water adducts.

Possible alternative experimental approaches to investigate the occurrence and distribution of clusters in the MALDI plume are postionization studies, flash photography, trapping plate experiments, and time-resolved (optical) spectroscopy. Handschuh et al. performed trapping plate experiments in which laser evaporated material was collected on silica wafers mounted 30 mm in front of the sample plate.[21] In this study, poly(ethylene glycol) (PEG) 3000 was mixed with 2,5-DHB in a molar ratio of 1:100. An N_2 laser with 3 ns pulse duration was employed for desorption. AFM micrographs of the collected material show the deposition of polyethylene/matrix clusters of up to 200 nm in width and 30 nm in height. The actual cluster size distribution was found to depend on the laser pulse energy. The size of 200×30 nm^2 of the largest clusters is comparable to the laser penetration depth of ~110 nm in 2,5-DHB. In addition to the particles, a smooth film coverage of the substrate was recorded, believed to result from the deposition of monomeric molecules. The results, therefore, indicate a MALDI plume composed of a mixture of PEG matrix clusters and monomeric molecules. Unfortunately, the A/M ratio of 1:100 as prepared by Handschuh et al. is relatively low and rather outside the normal MALDI A/M range for analyte compounds of

that size. It can, therefore, not be excluded that the high analyte concentration alone may have led to an enhanced aggregation of the poly(ethylene glycol) already in the preparation, and, further, to a general change in the ejection process. With respect to their physicochemical properties, PEGs, moreover, differ considerably from biomolecules. Experiments with lower A/M ratios or different analytes were not reported by Handschuh et al. Trapping plate experiments performed under conditions closer to the normal MALDI A/M-range would, however, appear as an easy implementable and very meaningful tool for further investigations.

Glückmann and Karas have recently discussed the relevance of cluster ejection and decay with respect to the ionization of analyte molecules in MALDI in a phenomenological "lucky-survivor" model.[126] This model accounts the observed MALDI ion species for by a statistical deficiency/excess of ions in individual clusters. Photoionization and subsequent photochemical processes were, moreover, discussed as major initial ionization processes. Glückmann and Karas stressed that the general observation of predominantly singly charged peptide ions in MALDI mass spectra is likely to be due to the charge reduction reactions of multiply charged clusters.

In a subsequent paper, Knochenmuss et al. argued that while such cluster reactions may add to the outcome, they do not form a principle prerequisite for the generation of the experimentally observed ion patterns. These authors rather see thermodynamically controlled intermolecular reactions in the expanding plume as the decisive factors and ascribe the high efficiency for the experimentally observed reaction channels to a high number of collisions in the plume as well as to high exothermicities of some of the reactions. They emphasized that secondary plume reactions alone therefore suffice to explain the predominance of singly charged (peptide) ions in UV-MALDI spectra.

In other work, these authors have determined the ionization potential (IP) of 2,5-DHB matrix[127,128] using a molecular beam technique and resonant two-photon ionization of monomeric matrix molecules and matrix oligomers. A striking feature of their results is that, although the ionization potential for the 2,5-DHB monomer is sizably higher than the energy of two photons at the most commonly used 337 and 355 nm laser wavelengths, the IP decreases considerably with the degree of DHB oligomerization. Kinsel et al. have, also with a molecular beam setup, furthermore shown that the IP can drop even more by a few tenths of eV if the clusters contain a high concentration of analyte molecules.[129] The results of these latter studies indicate that the resonant absorption of two photons at 337 or 355 nm, corresponding to 7.38 and 6.98 eV, respectively, can suffice to photoionize matrix−analyte aggregates.

Finally, Fournier et al. have recently reported (indirect) indications for cluster decay reactions in the MALDI plume from delayed extraction experiments.[130] As will be discussed in section V.A.I, this approach relies on difficult to control assumptions on the experimental conditions in the ion source, however.

I. Number of Ejected Analyte Molecules and Monolayers Per Laser Pulse

In view of the above discussion, the amount of material desorbed/ablated per laser pulse appears as an important criterion. Quite surprising, this aspect has not been addressed in much detail so far, however. Ejection of a monolayer or less of material per laser pulse, only, would for example be difficult to reconcile with any bulk-volume ablation model, whereas the removal of a large amount of material per laser pulse would make them very likely. Exact figures on the removed volume under controlled MALDI fluence and beam profile conditions are unfortunately not available. Some estimations can, however, be made on the basis of the estimated consumption of analyte molecules under controlled preparation conditions. This shall be attempted in the following section.

The minimum amount of analyte molecules necessary to generate a useful MALDI spectrum has been estimated by several authors: Jespersen et al., for example, used a micro-vial preparation protocol to approach this limit. 2,5-DHB, bradykinin, and cytochrome *C* were used as matrix and analyte compounds, respectively.[131] The amount of peptide molecules consumed per laser shot was determined to be on the order of 1 attomol. Keller and Li estimated the amount of desorbed substance P molecules desorbed from a αCHCA matrix from microspot preparation experiments to be about 1−10 attomol per laser pulse.[132] Vorm et al. also reported the detection limit for peptides to be in the low attomol range for αCHCA thin-layer preparations.[133]

Westmacott et al. estimated the number of detected peptide ions from their single ion counting experiments with a TDC detector to be within 20−100 at the common analogue MALDI ion threshold.[66] Converting this number to the amount of ejected neutrals is unfortunately not straightforward because of the largely unknown ionization efficiencies and fragmentation rates. As a conservative estimation, a fraction of 10^{-5}−10^{-4} intact analyte ions per desorbed analyte molecule may be assumed,[220] which means that again a low attomol amount of analyte molecules were desorbed per laser pulse, in agreement with the above values.

With an analyte-to-matrix ratio of 5×10^{-4} as used in the latter study, one then readily calculates that low femtomole amounts of matrix molecules are desorbed at the ion threshold. From the approximate thickness of a 2,5-DHB monolayer of ∼5 Å,[134] a surface coverage of about $\sim 5 \times 10^{-6}$ mol m^{-2} is further calculated. Within the flat-top laser spot of 200 μm in diameter as used in the study of Westmacott et al., 150 fmol of surface matrix molecules are then roughly forming the monolayer. Compared to ∼10 fmol by order of magnitude of matrix estimated to be desorbed per spectrum at ion threshold, this implies that only ∼0.1 monolayers are removed per laser pulse. Even if one takes the large uncertainty in these considerations into account, this rather low

value appears unlikely to account for any bulk volume ablation process. The study of Westmacott et al. has, moreover, shown that MALDI ions are even generated at substantially lower fluences (Figure 4).

Ion intensities, and presumably also the overall material ejection, do, however, rise steeply with laser fluence. For example, an increase of the fluence by about a factor of 2.5 above threshold (a value being typical for the upper limit of the meaningful MALDI fluence range in axial-TOF instruments) enhances the ion intensities of both postionized molecules and direct ions by a factor of 100−10000, depending on the actual matrix and irradiation conditions (Figures 3 and 4).[56,66] Assuming, for the sake of the discussion, a first-order linear relation between intensities and material removal, 3 (1.5 nm) − 300 monolayers (150 nm) were then desorbed/ablated at the elevated fluence. Typical laser penetration depths of 50−200 nm fall inside these values. Volume ablation is therefore likely to take place at the high side of the MALDI fluence range. Smaller laser spot diameters will lead to a similar "etch depth" closer to the ion threshold.[135] Although the above considerations are certainly very simplified, they demonstrate that, on one hand, a surprisingly large range of ion signal intensities and, probably, a likewise large range in the amount of removed material per laser pulse of several orders of magnitude results in surprisingly similar MALDI mass spectra. On the other hand, they indicate that the exact pathways of the MALDI process will depend strongly on the amount of deposited energy into the sample, making the idea of a general MALDI model for the whole usable fluence range rather obsolete.

IV. Material Parameters

A. Sample Morphology and Analyte−Matrix Interaction

It is common knowledge that the "right" matrix/analyte preparation constitutes one of the key requirements for a successful MALDI analysis. A too high load of salts or detergents in the preparation, for example, can deteriorate spectra quality considerably or even prevent analysis altogether.[136−138] A too high analyte-to-matrix ratio leads to a similar outcome.[58] The critical A/M ratio increases with molecular weight; for peptides in the low kilodalton mass range it is roughly in the range of $(1-5) \times 10^{-2}$.[58,139] These observations suggest that analyte−matrix preparations should be such that the "normal" crystal structure of the matrix lattice is preserved. Over a wider A/M range ion signal intensities increase generally nonlinearly with A/M,[58] a fact that hampers quantification in MALDI considerably. In semiquantitative approaches, internal standards of defined concentration and with physicochemical properties comparable to the analyte(s) of interest are, therefore, added to the samples and relative ion intensities are compared.[140−142]

The morphology of MALDI preparations has been investigated by optical microscopy,[14,39,143−147] including polarization and phase contrast measurements,[148] fluorescence studies,[149] confocal laser scanning microscopy (CLSM),[150,151] and by scanning electron microscopy (SEM).[147,152−155] These studies revealed that the morphology (habit) of an individual matrix compound will, besides on the aforementioned parameters (A/M-ratio, salts, detergents), in general depend on various further factors. Among these are the rapidness of solvent evaporation, the type of solvent, and the type and surface structure of the sample target. Compared to the above, these latter factors generally have a less strong influence on the mass spectrometric quality, however. The various common matrixes, moreover, express considerably different types of sample morphologies. A direct correlation between the morphology of a matrix and its MALDI-functionality is, therefore, not obvious.

The question whether analyte molecules have to be incorporated into matrix crystals for a successful analysis or whether a close surface contact, i.e., physi- or chemisorption, might already be sufficient, has been an issue of lively debate. A more comprehensive discussion of this problem can be found in a recent article by Glückmann et al.,[156] and is also the topic of very recent, yet unpublished work of these authors.[157] Analyte−matrix interaction has been studied by X-ray crystal structure analysis,[14,39,158] Raman spectroscopy,[152] mass spectrometric imaging,[159,160] and confocal laser scanning microscopy fluorescence investigations.[150,151] One of the important results from the X-ray crystal structure studies is that, as for the macroscopic morphology, so far no correlation could be established between the crystal structure of a compound and its suitability as MALDI matrix.

Strupat et al. have performed spectrophotometric experiments in which the incorporation of protein molecules (cytochrome *C*) into slowly grown, large 2,5-DHB crystals was recorded.[14] This study revealed that under these preparation conditions the A/M ratio of the mother liquor was approximately retained in the crystal. X-ray crystal structure analysis, moreover, revealed that the lattice crystal structure of neat 2,5-DHB was also maintained. Hillenkamp et al. previously coined the expression "solid solution" for the assumed homogeneous analyte incorporation.[12] In one of the initiatory studies, Beavis et al. have suggested that, upon crystal growth, sinapinic acid also incorporates protein molecules, but that for this compound analyte incorporation exclusively occurs at hydrophobic crystal faces.[158]

Recent SEM studies on (slowly) grown large 2,5-DHB crystals by Horneffer et al. indicate that the concept of a homogeneous solid solution for matrix−analyte preparations probably has to be revised as well.[155] This study showed that such crystals rather contain a high density of crystal defects, which were interpreted as trapped micro-inclusions of saturated mother liquor. Representative SEM micrographs from the work by Horneffer et al. are reproduced in Figure 7. The crystal defects were found to be of variable size, ranging from 10 nm to about 1 μm in diameter. The mean diameter and the number density of inclusions depend on the rapidness of crystal growth as well as on the size of the doping analyte molecules. The average diameter of the inclusions was found to decrease with increasing analyte mo-

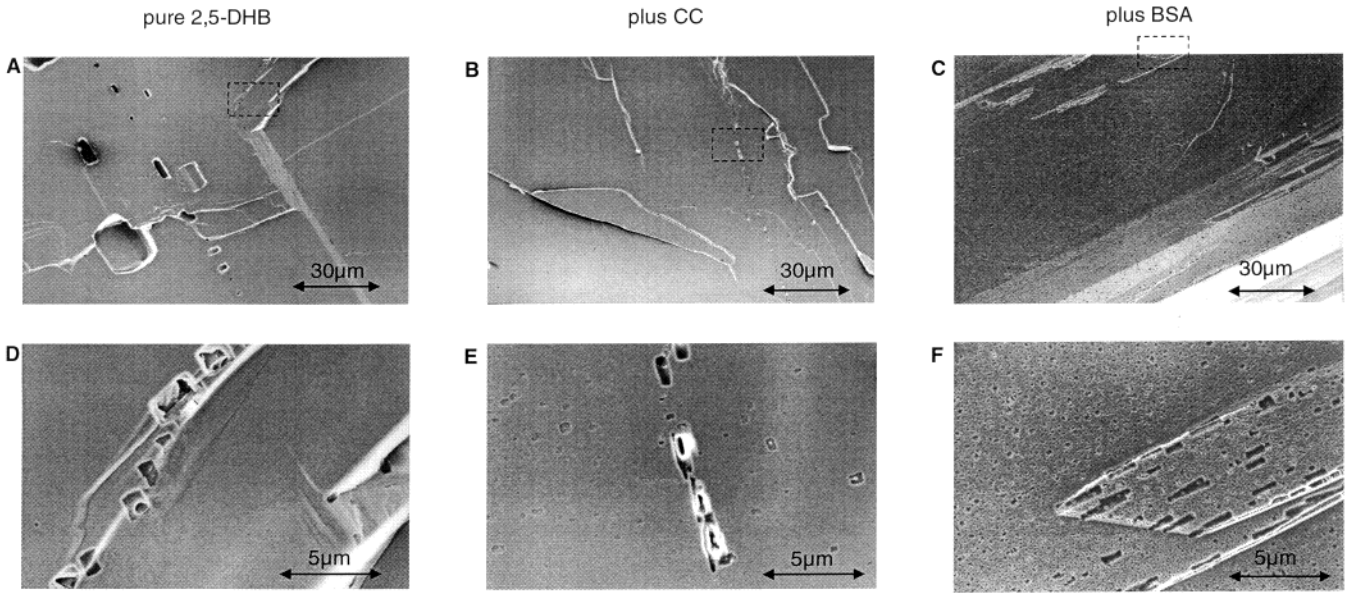

Figure 7. Scanning electron micrographs of opened inner faces of crystals of neat 2,5-DHB (A and D), doped with cytochrome *C* (B and E), and doped with bovine serum albumin molecules (C and F), respectively. D, E, and F are zoomed views of the marked area in A, B, and C, respectively. All crystals were grown from aqueous mother liquor containing 60 g/L 2,5-DHB and a protein-to-matrix ratio of 10^{-4}. (Courtesy of V. Horneffer; reproduced with permission from ref 155; copyright Elsevier Science, 2002).

lecular weight while the number density was found to rise. A decline in the size of the micro-inclusions was furthermore observed for forced speeds of crystal growth. Horneffer et al. concluded that a high density of very small inclusions is likely to be present in dried-droplet 2,5-DHB matrix preparations as well. Krüger et al.[161] and Brown and Durrant[162] have reported further indications for solvent inclusion in analyte−matrix preparations. 1-H NMR measurements indicated the presence of solvent in the investigation by Krüger et al., whereas Brown and Durrant used Karl Fischer-Titration to determine the residual water content in several slowly grown large matrix crystals. With the exception of 2,2′,4,4′-tetrahydroxybenzophenone, which was found to incorporate as much as ∼50−60 mole % of water, the other tested matrix crystals were determined to contain between 1.2 (αCHCA) and 4.3 mole % (2,5-DHB) of residual water.

The question whether analyte molecules possibly contained in the inclusions contribute to the overall ion yield or eventually even, in form of preformed ions, make out a major fraction can, at present, not be conclusively answered. Horneffer et al. pointed out, however, that similar cavities were also found in 2,6-DHB crystals although previous spectrophotometric measurements[39] as well as CLSM fluorescence studies with dye-labeled analytes[151] carried out by these authors had shown that this matrix does not exhibit any sizable incorporation of analyte molecules into its bulk crystal lattice. Furthermore, their investigation did not reveal any evidence for the formation of micro-inclusions in 3-HPA and αCHCA crystals. These authors, therefore, conclude, that neither the formation of solvent inclusions nor that of analyte incorporation into the bulk matrix-lattice do constitute in principle necessary requirements for a successful MALDI analysis. 2,6-DHB was even found to yield comparably good mass spectrometric results as the common 2,5-DHB isomer (inset table in Figure 1), provided that this matrix was prepared by fast evaporation of the solvent to form a microcrystalline structure with a large specific surface. The two studies[39,151] could not resolve whether analyte molecules may, if not in the bulk, yet be incorporated into a shallow surface layer of the 2,6-DHB microcrystals, which appears likely, or whether they are strictly physi- or chemisorbed.

Succeeding work by the authors, in which “dry” and “wet depositions” of analyte on matrix crystals were compared, showed that a sufficient rewetting of matrix surface layers, either by the analyte solvent itself, or by succeeding application of solvent, is a crucial prerequisite for “normal” MALDI.[157] In this latter study, dye-labeled insulin molecules were deposited on the matrix by electrospraying the analyte solution. Solvent evaporation from the droplets prior to deposition of the analyte molecules was controlled by using electrospray capillaries of different diameters. A rewetting of surface was indicated by fluorescence quenching (for pH-sensitive dyes), discussed by the authors to result from proton transfer from the acid matrix. Analyte mass spectra with reasonable quality could only be recorded from rewetted surfaces.

B. Preparation Protocols

Clear evidence that a superficial surface interaction can for certain analyte and/or matrix compounds, however, already be sufficient to promote desorption/ionization of high molecular weight analytes has been provided recently by studies in which samples were prepared in the form of pressed pellets of finely ground lyophilized powder of the compounds. This pellet preparation technique has been suggested by Skelton et al. for the analysis of analyte compounds that are not soluble in matrix-compatible solvents,[163] and has been utilized in a series of fundamental

experiments by Glückmann et al.[156] Because only moderate pressure is applied during the fabrication of the pellets, melting of samples can be excluded.

Despite the fundamental difference to the standard MALDI preparation protocol, surprisingly good mass spectrometric results were obtained for some analyte−matrix combinations. Glückmann et al. have, for example, reported that mass spectra of carbohydrates from carbohydrate-2,5-DHB pellets were even equal in quality to those obtained from standard dried-droplet preparations. Similar results were reported by Timpin et al. for the analysis of synthetic polymers of high molecular weight.[164] Glückmann et al. have emphasized that the pellet preparation yields significantly deviating results for different classes of analyte compounds, however. They noted that in contrast to carbohydrates, mass spectra of peptides were generally of inferior quality, in particular if these exceeded a few kilodaltons in molecular weight. Similar findings were noted by Wang and Fitzgerald.[165] Glückmann et al. discussed the differences between carbohydrates and peptides in the context of different ionization mechanisms by alkaline cationization, on the one side, and protonation on the other.

More recent work by Horneffer et al. revealed that the size of the microcrystals produced by the grinding of the lyophilized powders can play a very critical role in the analysis of peptides from such preparations but is less critical for carbohydrates.[157] Extended grinding of peptide-matrix mixtures in a ball-mill resulted in substantially improved mass spectra also for peptide samples and a 2,5- or 2,6-DHB matrix. Even cytochrome *C* ions (12 359 kDa) could then be detected out of a pellet preparation, although with notably degraded signal quality. For proteins, this size also appears to set the approximate limit: any attempts to generate bovine serum albumin (BSA) ions (66.4 kDa) from the pellets failed. An interesting finding from the study by Horneffer et al. is that the pellet preparation obviously works considerably different for different matrixes: In contrast to the two DHB isomers, αCHCA pellets were found to work only poorly for small peptides (bradykinin). Moreover, extended grinding was not accompanied by any sizable improvement in this case.

The relative insensitivity of MALDI to the sample morphology is reflected by the diversity in the applicable preparation protocols.[166] The most widely used dried-droplet and thin-layer protocols can, for example, be utilized with comparable success for most analyte compounds. In the dried-droplet method, matrix and analyte solutions are simply mixed and slowly air-dried to form analyte−matrix "cocrystals", whereas in thin-layer preparations volatile solvents such as acetone or acetonitrile facilitate a fast evaporation of solvent and the formation of homogeneous microcrystalline "films". Often, small volumes of analyte solution are only subsequently applied on top of these films. In that case, the use of aqueous solvents for the analyte, along with a less water-soluble matrix, e.g., αCHCA, ensures that only the upper layers of the matrix microcrystals are redissolved. Seeded film techniques[167] and preparations involving nitrocellulose[168] are further developments of the thin-layer technique, both promoting the formation of particular homogeneous films. Besides by the use of rapidly evaporating solvents, the generation of microcrystalline films can also be achieved by aero-[169] or electrospraying.[170] Preisler et al., recently, introduced a vacuum deposition method in which analyte/matrix effluent is supplied from a microcolumn.[171,172] This method was found to produce particularly fine microcrystals. It also forms an elegant means of "on-line" coupling of liquid chromatography (LC) or capillary electrophoresis (CE) with MALDI-MS.

The effect of solvent, buffers, and other detergents on the MALDI performance has been addressed in a large number of studies (e.g., refs 166, 173, and 174). In contrast to electrospray ionization (ESI) mass spectrometry, for which pure samples are a general requirement, MALDI is relative tolerant toward impurities. This tolerance can, in part, be associated with a chromatographic on-target cleanup effect:[173] upon solvent evaporation, impurities are excluded from bulk incorporation. In many cases, this exclusion also allows for a straightforward removal of "surplus salts" by simple washing steps.

More sophisticated purification steps, for instance, by ion exchange, chromatographic and electrophoretic methods, or membrane dialysis, generally improve the quality of mass spectra, however, and for many samples they are a must. MALDI nevertheless works often very well with crude extracts of biological tissue,[175−177] or even if pieces of biological tissue[178] and (single) cells[179−181] are directly mixed with matrix solution. In the latter cases, the low-pH of the matrix solution lyses the cell membranes and, therefore, leads to an at least partial release of the cell content. Hence, a "normal" cocrystallization with matrix will finally result. The direct analysis of crude extracts from (cultures of) viruses, bacteria, fungi, and spores has, moreover, been demonstrated.[182−185] Caprioli and co-workers have shown that even the formation of a thin matrix layer sprayed upon thin sections of tissue is sufficient to facilitate MALDI analysis of peptides contained in the tissue.[186−188] A critical factor in the preparation is, again, that matrixes are prepared sufficiently "wet", allowing for a release of analytes from the tissue into the matrix solution, and finally cocrystallization. Caprioli et al. have also described an additional step of contact-blotting of peptides/proteins onto C-18 coated polymer membranes for improved performance.[186−189]

MALDI analysis directly from thin polyacrylamide gels,[190] TLC plates,[191,192] and different membranes,[193] finally, constitute other examples in which rather crude than well-defined analyte−matrix preparations are involved. In the latter cases, the matrix is applied after the chromatographic separation of analyte compounds.

An altered crystallization and, as a result, probably likewise modified MALDI process is achieved if comatrixes are added to the preparation in high concentration. Frequently, small carbohydrates such as fucose or fructose,[194] or even multicomponent systems[195] are employed in this approach. The addition

of these co-matrixes has been found to reduce the metastable decay of co-desorbed analyte ions,[194] likely as a result of enhanced collisional cooling of analyte ions during plume expansion. This approach has, therefore, been found to be particularly helpful in the combination of MALDI ion sources with Fourier transform ion cyclotron resonance (FTICR) MS instruments,[194] which, because of the long source-cell transfer- and acquisition times on the order of seconds, require particularly stable ions.

Stainless steel targets are most commonly employed in conventional MALDI, although other metal substrates can be used as well as long as they are sufficiently inert to the matrix solution and, moreover, have a suitable surface tension with respect to the matrix-solvent system. The target surface morphology forms an important parameter for the crystallization process—commercial MALDI targets are, therefore, often fabricated with defined hatching. The use of nonmetal substrates has also been suggested, including Teflon,[196,197] nylon,[198] modified polymeric surfaces,[199] and paraffin wax.[200]

Schürenberg et al. have developed prestructured sample supports: defined, a few hundred micrometers wide hydrophilic (gold) domains within a hydrophobic sample coating (Teflon).[201] Upon evaporation of solvent, sample drops (~1 μL in volume are typically applied) shrink precisely on these "anchor spots", allowing for a considerable concentration effect and, hence, increase in sensitivity. Moreover, the reproducibility of signal intensities is generally improved.

In particular, the "sweet-spot" effect, a strongly irradiation-site dependent signal intensity variation for some matrix-preparations, is reduced by the miniaturization in sample preparation. The sweet spot effect is particular obvious in the analysis of oligonucleotides from a 3-hydroxy-picolinic acid (3-HPA) matrix. What distinguishes this matrix is not known. In an approach by Little et al. to improve the 3-HPA performance, nanoliter amounts of analyte solution are dispensed by a piezoelectric device, either premixed with matrix solution[202] or deposited on a preformed matrix layer spot on the target.[203] Although the mass spectrometric reproducibility is again greatly improved, the micromorphology of these nanoliter samples can still vary surprisingly strong and is depending on several factors, e.g., the matrix concentration in the dispensed volume. Figure 8 shows two examples of such nanoliter preparations, both applied with a piezo-dispenser onto 200 × 200 μm^2 wide hydrophilic domains. In the first case (Figure 8a), 16 nL of 300 mM of 3-HPA solution, containing 4.8 nmol of matrix, was dispensed. Figure 8b shows the preparation from a four times diluted solution. Here, 32 nL of 75 mM 3-HPA solution (2.4 nmol) were applied. Preliminary studies showed that the mass spectrometric results are probably not significantly correlated with these morphologies.

C. Sample Morphology after Laser Exposure

Some of the studies have also addressed the laser-induced damages. These experiments were naturally performed best on crystals with sizes larger than the laser spot. Strupat et al.,[14] Westman et al.,[153,204] Kampmeier et al.,[143] and Fournier et al.[106,205] used optical and scanning electron microscopy (SEM) to characterize the laser-induced surface modifications of either pure or analyte-doped large matrix crystals, grown from saturated solutions of 2,5-DHB[14,143] or sinapinic acid[106,205] (-analyte) solutions. αCHCA has further been investigated in a recent, at present yet unpublished study by Fournier et al.[206]

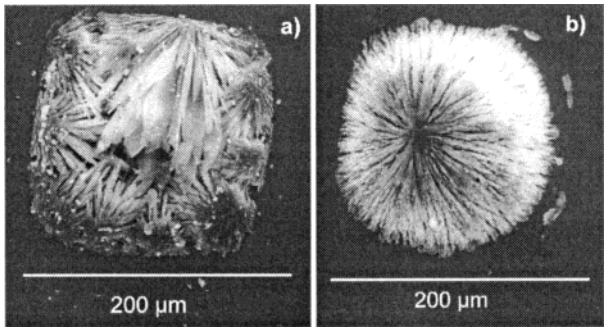

Figure 8. Scanning electron micrographs of two "nanoliter" preparations of 3-HPA matrix. Sample volumes were applied with a piezo dispenser onto 200 × 200 μm^2 wide hydrophilic domains. (a) Dispension of 16 nL of 300 mM 3-HPA solution (= 4.8 nmol of 3-HPA). (b) Dispension of 32 nL of 75mM 3-HPA solution (= 2.2 nmol of HPA). (Courtesy of F. Hillenkamp, 2002).

Figure 9 shows the results for large 2,5-DHB and αCHCA crystals from this latter study in which a flat top beam profile of 200 μm in diameter was used for irradiation. The SEM micrographs reveal several notable features: Few laser shots at fluences below the ion threshold were found to induce an "optical contrast" on the irradiated surface, in agreement with previous observations by Kampmeier et al. who used an alike system.[143] With increasing number of exposures at the same level of laser pulse energy, ablation crater formation became visible, increasing in depth with the number of exposures as well as with laser fluence. Within the material removal zone, the formation of substructures was observed in some studies.[106,130,143,206] These substructures are particularly evident when a uniform flat-top beam profile is utilized,[143,206] and exhibit distinct differences in appearance for the tested matrixes.[106,130,143,206] For irradiation of 2,5-DHB crystals (Figure 9a), the formation of cone-like structures has, for example, been observed by Kampmeier et al.[143] These cones were found to point in the direction of the impinging laser beam. Similar structures are also frequently observed for excimer laser processing of various types of materials such as polymers, metals, oxides and ceramics. [107,207−209] Although the crater formation proceeds expectedly faster with increased laser fluence, with respect to the microscopic picture of the crater morphology there is no notable indication for a change in desorption mechanism at the ion threshold.

A more detailed inspection of the irradiation zones in Figure 9 reveals another surprising aspect. Whereas in case of 2,5-DHB the ejection zone corresponds exactly to the size of the 200-μm-wide laser spot (elongated in one direction by the angle of incidence of 45°), in case of large αCHCA crystals this damage

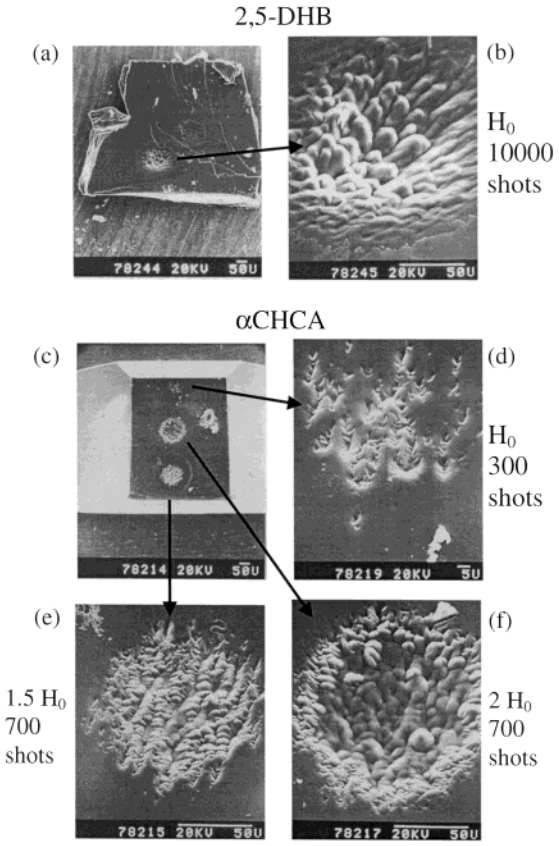

Figure 9. Scanning electron micrographs of large crystals of 2,5-DHB (a, b), and αCHCA (c−f), after irradiation with a nitrogen laser ($\lambda = 337$ nm; $\tau = 3$ ns). The nitrogen laser was coupled into a quartz fiber (FG-200-LAT, 3M, West Haven, CT) with an inner core diameter of 200 μm and the intensity profile on the end face of the fiber imaged 1:1 onto the sample to produce a homogeneous "flat-top" beam profile. The applied fluences and numbers of laser shots are indicated in the figure; H_0 denotes the ion threshold fluence. Micrographs b and d−f are zoomed views of the damage zones. (Courtesy of I. Fournier et al.[206]).

zone is considerably smaller. The boundary of the laser spot is, however, notable as a halo (e.g., lowest spot in Figure 9c). The reasons for these striking differences between the two matrix compounds are not known, yet; they are possibly related to the shallower excitation volume in the case of αCHCA (with a laser penetration depth of ∼30−50 nm compared to ∼110 nm for 2,5-DHB at the employed wavelength of 337 nm, as estimated from the solution absorption values).

Peculiar other differences between some cinnamic acid derivatives and 2,5-DHB or other matrix compounds have been reported before. Beavis et al., for example, were the first to note a distinct "hysteresis effect" for cinnamic acid matrixes;[205] consecutive laser exposures with low energy on a single spot are accompanied by a monotonic decrease in matrix and analyte ion intensities. Few exposures with high laser power bring the ion signals back to their full strength, however, and initiate a new cycle. Such effects are, for example, not notable for 2,5-DHB. Fournier et al. have studied this interesting phenomenon in more detail in two investigations.[106,205] In their recent work, these authors discuss matrix decarboxylation by pyrolysis, resulting in a shifted absorption profile, as a possible reason for the hysteresis effect.

An open question is, yet, to which extent the described results with large crystals are really representative for the polycrystalline standard MALDI preparations. The observation of smaller than laser spot size ejection zones for αCHCA in Figure 9 renders possible changes in the process with crystal size quite likely. Sadeghi and Vertes have, moreover, reported a strong dependence of the pathways of matrix volatilization on crystal size.[145] Sinapinic acid crystals with small dimensions in the micrometer-range were found to evaporate completely upon single laser pulse excitation and fluences in the MALDI range whereas larger crystals appeared to undergo a layer-by-layer "peeling".

V. Plume Dynamics

Measurements of the initial kinetic energies and energy distributions of the ejected ions, neutral molecules, and eventually particles, form the third group of fundamental investigations for a characterization of the MALDI process. A detailed knowledge of these parameters is moreover meaningful for further instrumental optimizations. A relatively large number of studies on the dynamic parameters of the MALDI plume has consequently been performed,[117,130,210−224] many more, moreover, on closely related systems of (direct) laser desorption ionization (LDI) of neat bio-organic compounds or other molecular substrates, e.g., refs 225−235. These experimental studies have further been supplemented by theoretical work,[113,236,237] and, more recently, by molecular dynamics (MD) simulations.[57,61,62,80,88,238]

A MALDI plume has to be characterized by several parameters. The first is its composition, i.e., the abundances of neutral molecules, oligomers, clusters, and finally molecular ions and oligomers, and fragments thereof. In a more comprehensive picture, the number densities of alkali atoms and ions and those of protons and electrons in the plume would also have to be regarded. Second, the temporal evolution of the material cloud is of interest, i.e., the pathways and time frames of condensed phase disintegration, the kinetics of the succeeding "hydrodynamic" motion and the extent of collisions between the plume components, the intermolecular reactions, including ionization and fragmentation, as well as the decay of molecular aggregates (clusters). After these initial processes have essentially ceased, the three-dimensional velocity distributions of the plume constituents will form the characteristic dynamic quantities.

All parameters have been investigated in one way or another in the past; the essential results of these studies shall be summarized in the following section. The data show that it is meaningful to differentiate between analyte and matrix, on one hand, and between neutral and ionic plume components on the other. They also reveal a complex overall picture, with some even contradictory details — which can at least in part be rationalized by differences in the concretely employed material and laser parameters.

An important aspect in the interpretation of all data is that collisions in the (dense) MALDI plume

inevitably lead to considerable dynamic changes during the material expansion. Several researchers have proposed that the "final outcome" of the expansion process—under conditions of laser-induced ejection with laser pulse durations on the order of nanoseconds and monolayers or more of ejected particles—will generally be governed by gas phase dynamics. A more detailed discussion of this important aspect is given in section V.B. Even in the "subhydrodynamic" case of very low desorption rates and plume densities kinetically controlled collisions will tend to modify the expansion. Therefore, initial velocity shall in the following be understood in the "usual" way as the free expansion velocity into the vacuum of the TOF spectrometer which the particles have acquired after essentially all interactions in the expanding plume are completed.

A. Mean Initial Velocities and Velocity Distributions

1. Ions

From the various parameters, the mean initial axial velocity of the ions is the one which has been most extensively studied, probably simply because it is also the "easiest" to access with regular time-of-flight mass spectrometers at hand. Considerably different axial velocities have, in fact, been reported for UV-MALDI ions, ranging from 200 ms^{-1} [211] to values considerably above 1000 ms^{-1}.[217] Berkenkamp et al. have recently pointed out that the lowest values were consistently reported in those studies in which a delayed extraction method (DEM, see below) had been applied, whereas investigations relying on field-free drift (FFD) measurements generally resulted in larger velocity values.[224] They emphasized that the observed differences between the FFD and DEM data may simply be due to the different measurement principles. These authors also discussed that too low values for the initial axial velocities may be obtained if the DE method is applied with nonoptimal experimental conditions. Their argumentation implied that the previously reported FFD data are more likely to reflect the true quantities.

Before further discussion of the data, a brief summary of the measurement principles shall, therefore, be given first. The employed techniques can essentially be arranged into two groups. In the delayed extraction method,[117,130,210,211,224] first described by Juhasz et al.[210] and Schürenberg et al.,[117] mean initial axial velocities are deduced from the change in the overall flight time upon variation of a delay applied between laser exposure and ion extraction voltage pulse in the ion source. Shape or width of the velocity distribution cannot be determined with the DE method. Prior to the onset of the extraction pulse, ions drift field-free in the ion source chamber. To deduce the mean initial velocities, the experimental flight time curves (as a function of the delay time) are fitted to a theoretical flight time equation in which the initial velocity is incorporated as a fit parameter. Berkenkamp et al. showed that this method is sensitive to the, likely large, number of collisions in the plume as well as to potential field-shielding effects caused by a high space charge density.[224] They also stressed that great attention must be paid to possible residual electric fields. Large ion-source stage distances and the use of long delay times were judged to considerably minimize the possible measurement error of the DE method. Most reported DEM experiments were, however, carried out with commercial instruments such as the Applied Biosystems Voyager DE in which rather short first ion stage distances on the order of 2−4 mm, only, are realized, optimal for a high sensitivity and mass resolution but less so for the velocity experiments. Karas et al. have, nevertheless, judged this measurement method as an "independent control measure" for an assessment of the desorption process.[161] The obvious differences between their data[211] (and also those of Juhasz et al.[210]) and those from several other investigations on comparable or even almost identical matrix and laser systems (2,5-DHB, αCHCA, and sinapinic matrixes,[117,213,258]), which yielded notably higher values, render this assessment at least problematic, however. More recent DEM measurements on 2,5-DHB by Berkenkamp et al.[224] and sinapinic acid by Fournier et al.[106] also confirm the higher average ion velocity values for desorption from these matrixes.

In the field-free drift methods, initial velocities have been deduced either entirely from the drift time in a field-free region,[223] from a comparison between the flight times with and without an accelerating field in a first ion source region,[212,213] or in orthogonal acceleration geometries in which ions were extracted perpendicular to the movement of their center of mass after passing through a field-free region.[214,233] In yet another variant, initial ion velocities were determined with a modified Wiley−McLaren ion-source setup.[217] Finally, a time-of-flight measurement utilizing an ion probe has also been reported.[239] A restriction of the FFD methods is, that due to the required long initial drift times, it will eventually discriminate against off-axis components. In general, the central axial plume component will be recorded, i.e., ions expanding at large angles may be lost. This method can, therefore, tend to overestimate the average velocity.

On the basis of the FFD values, it nevertheless seems evident that MALDI ions generally expand with rather high axial velocities on the order of several hundred to one thousand ms^{-1}. The data of Berkenkamp et al. showed that if DEM conditions are improved as discussed above, DEM and FFDM values also approach and overlap within the error ranges.[224]

Using a DE method, Glückmann et al. have recently reported distinctly lower mean ion velocities for carbohydrates (maltotetraose and chitotetraose) than for peptides (insulin).[211] The authors interpreted these differences in the framework of different ionization mechanisms of cationization by alkali ions versus protonation for the two analyte classes. They furthermore noted a change in initial velocities of peptide ions (insulin) when monosaccharides such as fructose were added in high concentrations to the preparation as "co-matrix".[240] Unfortunately, carbo-

hydrate ion velocities and ion velocities from preparations involving carbohydrates as co-matrix have hitherto not been reported by an FFD method, nor by an improved DEM. This appears very worthwhile in view of the implications the measurements by Glückmann et al. have. These authors have, furthermore, discussed a potential relation between the mean initial velocity of a matrix compound and its "softness" in terms of suppressing metastable analyte ion decay: They proposed that the higher the matrix velocity the cooler the plume will be. This would imply a particular effective collisional cooling for "fast" matrixes but further studies on this aspect are, in light of the above concerns, also necessary.

Some researchers have recorded a small but notable difference between the mean initial velocities of analyte and matrix ions, with slightly higher values for the matrix.[212,213,218] In other work, no clear difference was discernible, however.[211,214] The dependence of ion velocities on the analyte mass has generally been reported to be rather negligible, if detectable at all.[211,212,224] These findings, again, point to the high degree of entrainment of analyte ions in the matrix plume. The essential independence of mean analyte ion velocities on molecular weight leads to a first-order linear increase in the mean initial kinetic energies with mass. For large ions these can, therefore, approach values as high as several tens to one hundred eV.

Somewhat discrepant observations have been made with respect to the influence of the laser fluence on the velocities of molecules and ions. Glückmann et al., for example, did not observe any notable change in the mean initial velocities of ions upon variation of the fluence.[211] A similar independence on fluence has also been determined for the velocity distributions of neutral matrix molecules (section V.A.2). In distinct contrast, Spengler and Bökelmann reported an almost linear increase of the mean velocity of $(DHB-OH)^+$-fragment ions with laser fluence.[217] A particularly small laser spot size of 10 μm in diameter and accordingly high fluences were, however, used in these experiments and large single 2,5-DHB crystals irradiated. In comparison experiments with a "defocused" laser with a focal spot size of $\sim$150 μm in diameter, ion velocities were indeed found to be considerably lower. The influence of the fluence on the velocities was not studied/reported for the larger focal size.

Puretzky et al. noted a wavelength-dependent influence of the laser fluence on the velocity distributions of ions desorbed from a microcrystalline 3-HPA matrix. Two excimer lasers wavelengths of 193 and 248 nm were employed in this study. Their measurements were performed with a coaxial ion probe mounted a few centimeters in front of the sample target which did not allow for a mass spectrometric separation of ions. Only the overall flight-time distribution of all charged particles of one polarity were, hence, recorded including thus small cations as well as chemical noise fragments. At 248 nm, they recorded a relatively minor change in the shape of the ion velocity distribution. However, at 193 nm, a notable shift with fluence of the most probable velocity toward faster values was recorded.[220] These differences were interpreted as an enhanced contribution of direct photochemical bond breakage at 193 nm. Other studies that addressed the wavelength dependence but employed longer, more MALDI-typical wavelengths did not report a notable influence of the laser wavelength on the mean initial velocities.[210,211]

2. Neutral Molecules and Comparison of Neutral and Ion Velocities

The question as to which extent ion velocities coincide with those of the desorbed neutral molecules is a highly interesting one. Although both emerge from the same process, some substantial differences can be deduced from the reported studies.

Different methods have to be applied for the neutral plume components, for example, based on postionization in a defined volume above the sample surface. In this approach, the delay time between the desorption and the postionization laser pulse is usually varied and velocities are determined from the obtained ion intensity versus delay time distribution.[215] For a small enough ratio between the width of the postionization volume and its distance from the sample surface, this method also allows one to directly determine the velocity distributions. (Gated) laser induced fluorescence (LIF) techniques[220,239,241] as well as absorption spectroscopy[239] have, moreover, been used to characterize the UV-MALD(I) plume dynamics. With an ion-to-neutral ratio on the order of 10^{-3} or lower (section V.D) these latter measurements essentially yield the neutral velocities. Arrival time distributions in a volume element are the primary experimental data accessible with the experimental methods used in the latter studies. A detailed lay-out of the mathematical transformation from arrival times into velocity distributions has been given in various publications before, e.g., refs 242 and 243, and shall not be reproduced here.

Compared to the ions, sizably lower mean initial velocity values have generally been found for the neutrals. With the exception of the study by Puretzky et al.,[220] neutral and ion velocities have, however, not been determined in parallel for a given experimental system. Results from the latter study will, therefore, be discussed in more detail below.

Huth-Fehre and Becker determined the mean initial velocities of postionized gramicidin *S* (used as analyte) and ferulic acid (matrix) molecules to about 350 ms^{-1} for both species.[215] A quadrupled Nd:YAG laser (λ = 266 nm, τ = 5 ns) was employed for desorption in that work. Postionization was achieved with a vacuum-UV laser system by single-photon ionization. The fwhm of the (asymmetric) distribution was found to be $\sim$500 ms^{-1} for both analyte and matrix molecules; the distribution of the matrix molecules was, however, found to extend to higher values up to 1500 ms^{-1} in a low intensity tailing. Hence, the fastest neutral matrix velocities do cover the range of the ion velocities as determined in the aforementioned studies. Karas et al. determined the mean initial velocities of 2,5-DHB molecules with a similar postionization approach to $\sim$550 ms^{-1}.[244]

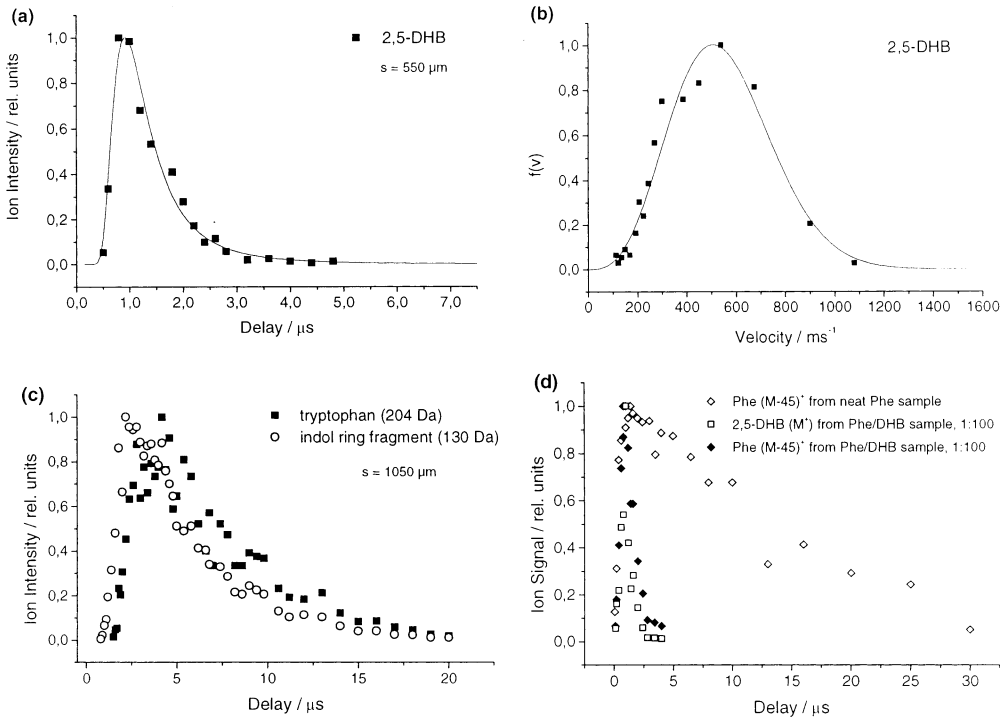

Figure 10. (a) Signal intensities of postionized 2,5-DHB molecules as a function of the delay time between the desorption (KrF excimer laser [EMG 102 MSC, Lambda Physik, Göttingen Germany]; $\lambda = 248$ nm; $\tau \sim 20$ ns; $\phi \sim 40-80$ μm) and the postionization laser (ArF excimer laser [EMG 50E, Lambda Physik, Göttingen, Germany], $\lambda = 193$ nm; $\tau \sim 20$ ns). The postionization volume was centered 550 μm above the sample surface. The width of the postionization volume was ~100 μm; the applied laser fluence was about the threshold for the direct generation of 2,5-DHB ions. (2,5-DHB data were recorded by B. H. Wang) (b) Velocity distribution as calculated from the data in (a). Solid lines are fits according to Equation 7 with a translational temperature of 1700 K. (c) Arrival time distribution of postionized tryptophan molecules. Desorption was achieved with the 248 nm-KrF excimer laser from a neat tryptophan sample and postionization in this case with an excimer laser pumped dye laser (FL 2002, Lambda Physik, Göttingen, Germany; $\lambda = 290$ nm; $\tau \sim 15$ ns). The postionization volume was centered at a distance of 1050 μm above the sample (width of the postionization laser beam waist, ~100 μm). (solid squares) signals of molecular tryptophan ions $M^{\bullet+}$ (204 Da); (open circles) signals of indol ring fragment ions (130 Da). The desorption laser fluence was adjusted to the threshold for direct generation of tryptophane ions. (d) Arrival time distribution of postionized phenylalanine and 2,5-DHB molecules, desorbed with the 248 nm-KrF excimer laser and postionized with the 193 nm-ArF excimer laser. (open diamonds) decarboxylated phenylalanine molecules (120 Da) from a neat phenylalanine (PheAla) sample; (solid diamonds) decarboxylated phenylalanine molecules (120 Da) from a PheAla: 2,5-DHB sample (1:100 molar ratio); (open squares) 2,5-DHB molecules ($M^{\bullet+}$, 154 Da) from the same sample. The applied desorption laser fluence was in both cases adjusted to about the threshold for the direct generation of phenylalanine ions from the neat sample. Compared to the experiments in (a)−(c) the distance of the postionization laser beam to the sample surface was less well defined in this case and smaller.

These results are displayed in Figure 10a and b; Figure 10a shows the intensity-delay time curve from which the velocity distribution, displayed in b was derived. The fwhm of the DHB velocity distribution is also about 550 ms^{-1}. A 248 nm KrF excimer laser with ~20 ns pulse duration was utilized for desorption in that work and an ArF excimer laser ($\lambda = 193$ nm; $\tau \sim 20$ ns) used for postionization. The focal spot size of the desorption laser on the sample target was ~40−80 μm in diameter. Fluences were adjusted to the ion threshold for direct generated (MALDI) ions. The velocity distribution was calculated from the arrival-time distribution in the postionization volume, centered at 550 μm above the sample surface (width, ~100 μm), according to eq 7 (section V.B). The figure shows that the experimentally determined distribution can be fitted well by a simple half-space Maxwellian velocity distribution ($u_0 = 0$) with a translational temperature of 1700 K (solid lines in Figure 10a,b). Huth-Fehre and Becker showed a similar fit for postionized gramicidin *S* analyte molecules in their study.[215]

Puretzky and Geohegan used a gated LIF technique to take time-resolved images of a 3-HPA MALDI plume. Using dye-tagged large protein molecules (deoxyribonuclease I, 29 kDa, A/M ~ 10^{-4}) and a second LIF wavelength, analyte and matrix molecule distributions could be distinguished.[220,239] A KrF excimer laser ($\lambda = 248$ nm, $\tau = 28$ ns, fwhm) and, in a second experiment, an ArF excimer laser ($\lambda = 193$ nm, $\tau = 22$ ns) were used for desorption along with a microcrystalline matrix preparation. Figure 11 displays the LIF results from the 248 nm study. The desorption excimer lasers were used unfocused, which resulted in a homogeneous but large millimeter-sized laser spot; the applied fluences were on the order of 100−700 J m^{-2}.[239]

Figure 11 reveals forward-peaked distributions for both plume constituents. Compared to the matrix, the expansion of the co-desorbed biomolecules is notably sharper.[220] A high degree of convergence of axial analyte and matrix velocities is, hence, observed, whereas the radial velocities of the biomolecules remain much lower. Puretzky and Geohegan inter-

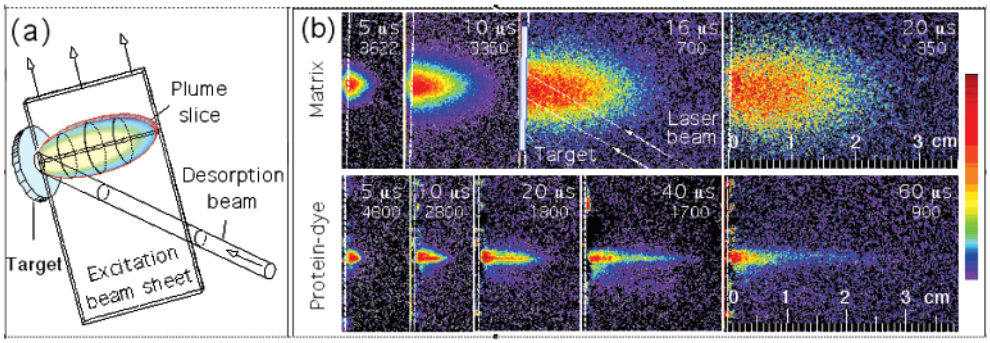

Figure 11. (color) (a) Schematic of MALDI plume irradiation geometry (as used in ref 220). Desorption was induced with a KrF laser beam (3.1×3.6 mm^2 elliptical beam spot). LIF excitation utilizes a sheet beam from a second laser fired at variable time delay after the desorption laser pulse. (b) CCD images (100 ns gate width, opened 50 ns prior to the LIF laser pulse) of LIF from matrix and dye-tagged protein molecules. Each image represents a different desorption event. Time delays after desorption and the maximum intensity (red, see palette) of each image are listed. Dashed lines show the target position. (Upper row) LIF images of 3-HPA matrix vapor plume (excitation: 308-nm XeCl, 1.6×35.0 mm^2 rectangular beam spot); (lower row) LIF images of TMR-dye labeled DNase I protein (3.1×10^{-5} M) embedded within 3-HPA matrix and desorbed with a KrF laser (excitation: 532 nm, second harmonic of Nd:YAG laser, 0.3×35 mm^2 beam spot). A 550-nm long-pass filter was used to cut off 532 nm scattered laser light. (Courtesy of A. A. Puretzky; reproduced with permission from ref 220; copyright American Physical Society, 1999).

pret this "plume sharpening effect" as the result of a high number of collisions with a lacking radial frictional interaction of the biomolecules with light matrix molecules. The average axial neutral velocities were found to be between 600 ms^{-1} for a desorption laser wavelength of 248 nm and 800 ms^{-1} for the 193 nm desorption laser wavelength.[239] A certain drawback in the study by Puretzky et al. (as well as in the above-described postionization work) is the employment of the 248 nm excimer lasers with relatively long pulse durations of $\geq$20 ns, which might shift the process conditions to fall somewhat outside those of common UV-MALDI. 3-HPA as employed as matrix in the work by Puretzky et al., moreover, has a rather low solution absorption at 248 nm, although an altered spectral profile with higher absorption at 248 nm has been reported in the article for the microcrystalline solid state 3-HPA preparations.[239] Moreover, fluences have been applied which for these absorption values can be expected to fall quite well within the normal MALDI range. The setup did, however, not allow for a mass spectrometric control. The large millimeter laser spot size employed in the investigation by Puretzky et al. could furthermore alter the gas dynamic expansion significantly. A similar experiment with more common MALDI irradiation conditions, employing for instance a (focused) nitrogen (λ = 337 nm) or a frequency-tripled Nd:YAG laser (λ = 355 nm), would therefore appear as highly interesting.

As noted above, in an additional experiment Puretzky et al. also determined the velocities of the ionic plume constituents by means of a coaxial ion probe, mounted 5.4 cm in front of the sample. Although this setup did not allow a differentiation between ion species, the results show that the leading edge of the neutral velocity distribution fully overlaps with the ion distribution. Ions are, hence, essentially found in the front part of the expanding plume. From their absorption measurements at different excitation wavelengths, Puretzky et al. concluded that the front part of the plume also contains the internally hottest 3-HPA molecules, indicated by a large abundance of 3-HPA fragments with modified absorption profile.[239,258] These results, therefore, suggest that ionization in the MALDI plume may be favored by the presence of internally hot matrix ions or that of matrix fragments.

Indications for a forward-peaked ion distribution have also been described in several other studies. Zhang and Chait have, for example, reported a "jet-like desorption" of peptides from αCHCA and sinapinic acid matrix preparations.[213] They also noted a considerably stronger forward-peaking for the co-desorbed biomolecules than for the matrix ions. The authors found the mean radial velocities to be sizably lower than the axial ones, namely, ~140 ms^{-1} for the co-desorbed dynorphin 1−13 analyte, only, and ~240 ms^{-1} for the αCHCA dimer, respectively, which has to be compared to 660 and 850 ms^{-1}, respectively, for the axial components. Similar, results were obtained in this study for a sinapinic acid matrix. Zhang and Chait, moreover, reported some dependence of the radial velocities on the kind of the preparation—single large crystals and thin-layer preparations had been compared. Spengler and Bökelmann have also noted a forward-peaked distribution for 2,5-DHB matrix ions, desorbed from single large crystals.[217] As noted above, a rather small laser spot on the order of 10 μm and a high laser fluence were, however, applied in this latter work.

Dissimilar results have been reported regarding the "shape" of the MALDI plume, a quite relevant and probably somewhat disregarded parameter for an assessment of the MALDI process. A "bimodal plume" characteristic with a "tailing" toward high velocities can for example be deduced for the ferulic acid matrix velocity distributions in the postionization study by Huth-Fehre and Becker.[215] For the entrained gramicidin *S* analyte molecules such a tailing is much less obvious, if present at all. From a detailed analysis of Figure 11 from the study by Puretzky et al., a bimodal plume characteristics can also be extracted for the analyte molecules, though that is in this case less obvious for the matrix.[220]

Zhigilei and Garrison determined in their MD work an essentially "smooth" velocity distribution for matrix molecules if ejection occurred in the "desorption regime". This could reasonably well be fitted by a Maxwellian velocity distribution on a single stream velocity with an u_0 of 375 ms^{-1} (eq 7). The "plume temperature" according to the Maxwell-part of the distribution was found to be about that of the peak sample temperature. Some distinct deviations between the MD values and the fit were noted, however, especially toward the high velocity side. Zhigilei et al. found the MD velocity distribution to change to a highly asymmetric one upon transition to the "ablation regime". The fasted molecules were now found to approach values as high as 2000 ms^{-1}. These results suggest that the plume shape may in fact serve as an indicator for a differentiation between sublimation/evaporation-like processes, on one hand, and phase explosion, on the other. As discussed above, a major obstacle in the interpretation of the MD results and comparison to corresponding experiments are the distinct limitations set on the excitation (150 ps were used) and overall simulation times ($\sim$1 ns) as well as on the spatial scales ($\sim$1 μm).

In contrast to the above works, Beavis and Chait,[212] Zhang and Chait,[213] and Pan and Cotter[214] have in their measurements on ions not recorded any indications for a bimodal or distinct asymmetric plume characteristic. A bimodal plume shape is also not notable in the 2,5-DHB molecule velocity distribution of Figure 10a,b.

Unpublished postionization work performed by the author on some other matrix and various other small organic compounds revealed that the actual plume development, however, depends substantially on the physicochemical properties of the compounds. The same 248 nm excimer desorption laser as above for 2,5-DHB was employed in these experiments. The tested matrix compounds, sinapinic acid, vanillic acid, and nitrobenzyl alcohol, were found to essentially exhibit unimodal expansion characteristics such as 2,5-DHB (data not shown). However, direct laser desorption of other small organic compounds of similar size (e.g., amino acids, dipeptides) was found to eventually result in considerably broader, asymmetric velocity distributions. Preliminary results also showed that nicotinic acid, the historically first matrix compound, seems to exhibit deviations from the unimodal plume shape, with an extension to both slow and fast velocity components (data not shown).

Figure 10c displays the intensity-delay time distribution of the amino acid tryptophan (204 Da; prepared as neat sample) as an example for the occurrence of significantly "broadened" distributions. Postionization was in this experiment achieved with an excimer laser pumped dye-laser tuned to 290 nm ($\tau \sim$ 15ns), desorption as above with the 248 nm excimer laser. Note that different distances between the postionization laser beams and the sample surfaces have been used in the different experiments displayed in Figure 10; these are indicated in the figure caption.

A clearly different plume expansion characteristic is visible for tryptophan with postionization signals being recorded for delay times exceeding 20 μs. It seems reasonable to assume that these "slow" plume components originate either from the ablation of large, slow clusters with velocities as low as $<$50 ms^{-1}, or, in an alternative explanation, from a prolonged ejection of molecules. The different mechanisms for laser ejection of 2,5-DHB and tryptophan can possibly be explained by the sizably higher cohesive lattice energy of tryptophan, indicated by a high melting point (mp) of $\sim$290 °C at 1 atm (equilibrium heating at 1 atm leads to decomposition). This value can be compared to the mp of 2,5-DHB of 205 °C and that of some of the other tested compounds: phenylalanine, 270 °C (decomposes as tryptophan); alpha-cyano-4-hydroxycinnamic acid, $\sim$240 °C; nicotinic acid, 235 °C; 3-hydroxypicolinic acid, 220 °C; caffeic acid, 218 °C; 2,5-DHB, 205 °C; sinapic acid, 200 °C; ferulic acid, 170 °C; nitrobenzyl alcohol, 32 °C (all values are for $p = 1$ atm). It seems worthwhile to address the role of the cohesive lattice energy in more detail, for instance, by future MD simulations.

A peculiar feature in the LDI process from tryptophan, so far only observed for this compound and some tryptophan-containing dipeptides, but not, for instance, for other tested indol derivatives like, e.g., indol-3-acetic and -3-butyric acid, is the observation of notably faster indol ring fragments at 130 Da (Figure 10c). These ions could be the result of photoionization of indol ring (fragment) molecules which were already produced during the desorption step. The data suggest that this fragmentation step would then lead to a considerable increase in velocity. The hypothesis of a photochemical bond breakage at the indol ring is supported by the observation made in other studies of laser-induced electron transfer from the indol ring chromophore to the electrophilic carboxyl group of the amino acid part, with successive change of the electronic coordination to a nonbinding state.[245,246] Alternatively, indol ring fragment ions might be generated from internally particularly hot and fast neutral tryptophan molecules forming the leading edge of the expansion plume. However, the complete absence of any intact $M^{\bullet+}$ signal of tryptophan at short delay times would then be difficult to understand.

Figure 10d shows that also the "matrix effect" can be followed very nicely by the postionization approach. In this case, phenylalanine (165 Da) was used as "analyte" and the 120 Da immonium fragment, prominent in the postionization mass spectrum, used for data evaluation. Whereas, if prepared as a neat sample, phenylalanine molecules were, alike tryptophan, detected in the postionization volume at delay times as long as 30 μs, the delay time vs intensity distribution changed completely if phenylalanine was mixed with 2,5-DHB in a 1:100 molar ratio. In this case, the velocities of postionized phenylalanine approached those of the matrix.

Elevation of the desorption laser fluence led to further relative enhancement of tryptophan and phenylalanine postionization signals at long delay times if these compounds were prepared as neat

samples (data not shown). Tested was a fluence range from ion threshold to about 1 order of magnitude above. The most pronounced fluence effect was found for highly viscous α-tocopherol (vitamin E) preparations, resulting in postionization signals at delay times as high as 100 μs for high fluences (data not shown). In no case was the higher laser fluence accompanied by the detection of faster molecules. In contrast to these compounds, the relative intensity-delay time distributions of 2,5-DHB and those of the other tested matrixes (including nicotinic acid) were not affected by an increase in the desorption laser fluence.

The results of the last paragraphs illustrate that the mere recording of ion velocities will in most cases not suffice for a sound characterization of the plume expansion, in particular, not if these experiments return average axial ion velocities, only. Further investigations with either postionization or LIF techniques appear therefore very worthwhile to elucidate also the potentially different mechanisms of desorption/ionization for carbohydrates and peptides/proteins.[211] A rather interesting question is, furthermore, whether the observed differences in the postionization experiments do possibly reflect relevant matrix properties, e.g., in terms of a sufficiently weak intermolecular binding strengths of suitable matrixes, or a sufficiently fast cluster decay.

B. Gas Phase Dynamics

Velocities of atoms, molecules, and particles, generated by short-pulsed laser excitation from diverse substrates are very generally found to considerably exceed those calculated for equilibrium surface evaporation, even for very simple systems. On this background, the high values in MALDI do not come as a surprise. Frequently, the high mean axial values in MALDI are nevertheless seen as a proof or disproof for/against certain phase transition models, for example, as a disproof of surface sublimation, a likely to rush assumption. Several researchers have addressed the above findings and attributed the enhancement of axial velocities to a kinetic transformation of radial and internal energy into axial particle movement (e.g., refs 247−251). Noorbatcha and Lucchese[252] and Cowin et al.[253] have shown that a notable change in the three-dimensional plume distribution of free expanding gas plumes occurs already in the case of monolayer or submonolayer desorption of simple molecules, and that already in these cases a Knudsen layer will generally be fully developed. In fact, such "hydrodynamic" processes can be assessed to be particular effective for the MALDI case, given the rapidness of the phase transition, the high number of ejected particles, the large aspect ratio (i.e., size from which ejection takes place vs the ejection depth) and the large collision cross sections of the compounds. One fundamental result of the hydrodynamic theory is that the final velocities are to a wide extent solely determined by the gas-phase processes. In other words, molecules and particles have lost (part of) the memory about their origin.

Several researchers have consequently described the MALDI plume expansion as supersonic. Knochenmuss, for example, adopted the classical theory of adiabatic isentropic supersonic (molecular beam) expansion[254] to calculate the initial acceleration of MALDI plumes.[98] Combining the plume expansion dynamics with the density-dependent rate equations for ionization reactions he concluded that ions will preferably "survive" reneutralization reactions in the front part of the plume, in agreement with the above experimental results. A particular feature of the UV-MALDI case, not accounted for by the classical molecular beam theory is, however, that the phase transition in MALDI is time-wise a very short event. It is furthermore "self-determinating" to a certain extent, caused by either phase explosion, i.e., by the instantaneous expel of an entire excited volume, or by effective evaporative cooling of the surface due to the consumption of latent heat by the vaporization. Moreover, ample reactions inside the plume like cluster decay and intermolecular reactions will lead to considerable deviation from any isentropic case.

Puretzky and Geohegan have applied gas dynamics theory to include the case of bicomponent MALDI plumes. They found that their experimental data could be fitted in good agreement with theoretical predictions if some reasonable assumptions on gas-phase quantities (e.g., on the adiabatic exponent c_p/c_v) were made.[220] Puretzky and Geohegan[220] and Chen et al.[247,255] emphasized that the "source" from which desorption in MALDI takes place is not stationary—in contrast to, for example, thermal desorption from a surface held at a constant temperature—but rather expanding dynamically as a result of laser heating. This "dynamic source effect" furthermore accelerates the expansion in the direction of the surface normal.[247,255]

Several researchers have proposed that because of the "jet-like" expansion the axial velocity distribution of laser ejected particles should be described by a function composed of a half-space Maxwellian and a stream velocity, u_0, of the general form:[242]

$$f(v) \sim v^3 \exp\left(\frac{-m(v-u_0)^2}{2kT}\right) \qquad (7)$$

where m is the mass of the molecule or ion, v is the particle velocity, u_0 is the center of mass stream velocity, k is Boltzmann's constant, and T is the plume temperature. To include the radial component, elliptical velocity distributions of the form

$$f(v_x, v_y, v_z) \sim \exp\left(-\frac{mv(v_z-u_0)^2}{2kT_z} - \frac{mv(v_x^2+v_y^2)}{2kT_{xy}}\right) \qquad (8)$$

with two different characteristic "temperatures", T_{xy} and T_z, for the radial (xy) and the axial direction (z) have also been introduced.[248,256,257] Notably, best fits of eq 7 to the velocity distributions of neutral molecules as obtained in the postionization and LIF experiments were found for rather low values of u_0, however,[215,258] or even for $u_0 = 0$ (Figure 10a,b). High "translational temperatures" on the order of 1000 K follow from these pure Maxwellian fits.

Zhigilei et al. suggested that, because of the free expansion character of the system, a set of stream velocities rather than a single u_0 will account more correctly for the expansion process.[57] In their MD simulations, the final velocity a molecule acquires upon ejection was calculated to depend to first order linearly on the sample depth from which that particle was released. The highest velocities were, hence, found for volume elements close to the original surface. Equivalent results were reported by Knochenmuss from his molecular beam plume expansion calculations.[98] However, comparing theoretical and experimental data, quite large differences are notable which suggests that further refinements in the theoretical approaches are necessary.

C. Internal Energies

Several researchers have proposed that expansion cooling in the MALDI plume leads to a stabilization of labile analyte ions, and therefore forms an essential reason for the functionality of MALDI. The recently reported benefits of high-pressure MALDI sources[259] or collisional damping interfaces[260] for the analysis of particularly labile analyte substances can further be attributed to collisional cooling of analyte ions, in this case by collisions with small background gas atoms. Vertes et al. have addressed these aspects in hydrodynamic calculations and showed that a considerable drop in the mean internal energy of co-desorbed analyte molecules can indeed be expected within a few tens of nanoseconds after desorption.[113] The consumption of the latent heat of sublimation plays a significant role in these considerations.

Some conclusions on the internal energies of laser desorbed 3-HPA matrix molecules can be drawn from the absorption spectroscopy measurements by Puretzky et al.[220] As noted above, these authors determined an increased abundance of hotter matrix molecules in the front part of the expanding MALDI plume (section V.A.2). Mowry and Johnston performed postionization studies with small, primary and secondary alkylamines as analyte compounds.[73] These authors determined that the internal energies of the desorbed alkylamine molecules corresponded roughly to the "sublimation temperature" of the different tested matrixes from which they were co-desorbed. An open question remains as to how far these results can be transferred to substantially more complex typical MALDI analyte compounds. Stevenson et al. employed low-energy collision-induced dissociation (CID) in an FTICR-cell to estimate the internal energy of dinucleotide ions desorbed from different common matrixes.[261] In contrast to the results of Mowry and Johnston, Stevenson et al. did not find any correlation between the internal energies of the analyte ions and the sublimation temperature of the matrix. Instead, their measurements indicated a strong correlation with the gas-phase basicities of the matrix anions. Stevenson et al. concluded that gas-phase proton transfer reactions are, therefore, likely to play a decisive role in MALDI analyte ion formation. All in all further spectroscopic investigations are clearly pending to characterize the "temperature" of the MALDI plume and in particular the internal energies of analyte molecules and ions.

D. Ion-to-Neutral Ratio

An assessment of the ratio between molecular ions and neutral molecules in the MALDI plume is anything but straightforward. This is not at least due to the essentially unknown ratio of fragmented versus intact ions as well as the generally not well-known instrumental transmission and detection efficiencies. It is, therefore, in general not evident whether an ion signal is low in intensity simply because only few ions have been generated or whether rather a large fraction is lost by fragmentation prior to detection. Furthermore, one has to differentiate between ion-to-neutral ratios of analyte and matrix molecules. For typical MALDI conditions, these two quantities must be expected to be sizably different.

Ion counting and postionization data can at least help to set some limits on the above figures. Following the estimations made in section III.I on the number of molecules and ions desorbed at ion threshold fluence, a ratio n_i/n_o of between 10^{-4} and 10^{-3} can be deduced for peptide ions, where n_i is the number of (intact) desorbed molecular ions, and n_0 that of neutral molecules. Mowry and Johnston estimated the ion-to-neutral ratio for the alkylamine analytes postionized in their study to $\leq 10^{-4}$.[72] Puretzky et al., finally, estimated the overall ion-to-neutral yield (sum of analyte and matrix species) to an n_i/n_0 of $\sim 10^{-5}$ from their comparison studies with absorption spectroscopy and ion probe measurements.[220] Values between $10^{-5}-10^{-3}$, as set by these investigations, seem therefore likely to span the actual n_i/n_0 range in MALDI.

Several factors are likely to moreover have a considerable influence on the ion-to-neutral ratio in a concrete experiment, among which will be the irradiation parameters (e.g., the laser fluence; Figure 3), the preparation conditions (e.g., the analyte-to-matrix ratio[58]), and the physicochemical properties of analyte and matrix. Attempts to increase the ion-to-neutral ratio by adding proton donor agents to the preparations have generally been found to not result in an enhancement for those compounds which are preferentially detected as protonated species (like peptides and oligonucleotides). The addition of metal salts or other cationizing agents can, on the other hand, sizably enhance the ion yield for carbohydrates[262] and synthetic polymers.[263,264]

VI. Concluding Remarks and Outlook

This review summarized investigations performed on the MALDI desorption process within about the last 15 years. These fundamental studies have illustrated various facets of a complex process. One of the most striking findings is probably the surprisingly broad range of material and laser parameters for which MALDI works. A wide range from very simple to very complex analyte compounds of diverse chemical nature can be analyzed from a variety of matrixes and, furthermore, in an extraordinarily molar A/M concentration range of $< 10^{-9}$ to $\sim 10^{-2}$.

For a given, say, not too low A/M ratio, a similar broad range is found for the number of ions generated per laser pulse, from below one intact ion on average at the very low fluence side to several tenthousand at elevated fluences. This span corresponds to widely different amounts of ejected material. The MALDI process in general has, therefore, a strong dependence on the irradiation and material parameters and spans from molecular desorption at the very low fluence side up to that of volume ablation by phase explosion at elevated fluences.

Successful MALDI analysis nevertheless requires the attention to several key factors, of which a sufficiently rapid phase transition from the condensed to the gas phase is a particularly crucial one. IR-MALDI and photoacoustic desorption studies even imply that this fast phase transition "alone" can in principle provide for an environment sufficient to result in the generation of ionized gas phase molecules. Also rapid heating by surface-MALDI allows desorption/ionization of a range of analyte compounds, but the limitations on the upper mass limit of the latter MALDI mode clearly demonstrate that further factors are indispensable to allow for a sufficiently soft desorption and ionization of labile analyte species. The thermodynamic properties of the matrixes are, therefore, believed to play a decisive role in the final outcome. A "sufficient" analyte−matrix interaction in the sample is another crucial factor. Finally, gas phase interactions as indicated by the dynamic properties of the expanding plume with its high velocities and highly forward-peaked expansion characteristics must be regarded to also play a central part in the overall process. An important "side effect" of the plume expansion is cooling of the internal degrees of freedoms of the analyte molecules. Whereas in the most common vacuum-MALDI sources this beneficial effect is achieved quasi within the process, new developments of high-pressure MALDI sources demonstrate that it can be enhanced by controlled inlet of background gas. Investigations addressing high-pressure MALDI have so far essentially concentrated on the analytical potential. Due to the rapid cooling, high-pressure MALDI sources have been found to be much less sensitive to the application of high laser powers. In fact, fluences considerably beyond the normal vacuum-MALDI window are often applied to maximize ion signal intensities. Very probably, high fluence, high-pressure MALDI, therefore, further extents the range of possible pathways of phase transition.

A number of questions are raised by the results depicted in this article. Several of them can be transformed into a "wish list" for future experiments. Some, in the personal view of the author, especially interesting ones shall be sketched in the following:

A relatively straightforward but very meaningful experiment would be, a somewhat surprisingly still pending, more meticulous investigation of the role the desorption laser wavelength has in MALDI, e.g., in view of the course of threshold fluences with wavelength and of that of the mass spectrometric matrix (and analyte) ion patterns. Photochemical as well as photoionization pathways may become visible by changing the laser photon energy. Ideally, such experiments would also include postionization of neutral molecules to differentiate between neutral material ejection and ionization to some extent. A possible optimization of the analytical performance for certain matrixes might turn out as a highly welcomed side effect.

Further investigations on the likely pathways for the phase transition in MALDI, in particular with respect to a differentiation between sublimation/evaporation and phase explosion, are clearly highly desirable. Several possible approaches have been discussed in this article. A relatively straightforward one would be the extension of previous trapping plate experiments with standard MALDI preparations and the use of cooled trapping plates to enhance sticking coefficients and prevent thermal resublimation. Temporal-spatially resolved spectroscopic recording of the plume expansion and in particular that of cluster ejection is considerably more demanding but would also be of even higher interest. An extension of the discussed absorption spectroscopic, LIF, as well as the postionization work to typical MALDI conditions with 337 or 355 nm wavelengths and pulse durations in the low nanosecond range also appears as very meaningful.

Some of the suggested experiments would very likely also shed more light onto the barely understood spot-size effect. Refined measurements on the overall material ejection and its dependence on the irradiation parameters using microbalance or photoacoustic detection schemes would supplement such investigations more than advantageously. The obvious differences between MALDI of peptides/proteins (and oligonucleotides), on the one hand, and carbohydrates (and synthetic polymers), on the other, clearly demand further clarification, as do the apparent contradictions in the reported values of MALDI ion velocities. In view of the discussed differences between neutral and ion velocities and the possible relevance of the plume shape, determination of the three-dimensional distributions rather than the average velocities should generally be looked for.

VII. Note Added after ASAP Posting

In the original version posted ASAP 1/24/2003 in paragraph 10 of Section V.A.2. the mention of eq 37 should have stated eq 7. The correct version was posted 1/28/2003.

VIII. References

(1) Karas, M.; Bachmann, D.; Hillenkamp, F. *Anal. Chem.* **1985**, *57*, 2935.
(2) Karas, M.; Bahr, U. *Trends Anal. Chem.* **1986**, *5*, 90.
(3) Karas, M.; Bachmann, D.; Bahr, U.; Hillenkamp, F. *Int. J. Mass Spectrom. Ion Processes* **1987**, *78*, 53.
(4) Karas, M.; Hillenkamp, F. *Anal. Chem.* **1988**, *60*, 2299.
(5) Karas, M.; Krüger, R. *Chem. Rev.* **2003**, this issue.
(6) Knochenmuss, R.; Zenobi, R. *Chem. Rev.* **2003**, this issue.
(7) Hillenkamp, F.; Unsöld, E.; Kaufmann, F.; Nitsche, R. *Nature* **1975**, *256*, 119.
(8) Vastola, F. J.; Mumma, R. O.; Pirone, A. J. *J. Org. Mass Spectrom.* **1970**, *3*, 101.
(9) Posthumus, M. A.; Kistemaker, P. G.; Meuzelaar, H. L. C.; de Brauw, M. C. *Anal. Chem.* **1978**, *50*, 985.
(10) Stoll, R.; Röllgen, F. W. *Org. Mass Spectrom.* **1979**, *14*, 642.

(11) Boesl, U.; Weinkauf, R.; Weickhardt, C.; Schlag, E. W. *Int. J. Mass Spectrom. Ion Process.* **1994**, *131*: 87, and references therein.
(12) Hillenkamp, F.; Karas, M.; Beavis, R. C.; Chait, B. T. *Anal. Chem.* **1991**, *63*, 1193A.
(13) Beavis, R. C.; Chait, B. T. *Rapid Commun. Mass Spectrom.* **1989**, *3*, 233.
(14) Strupat, K.; Karas, M.; Hillenkamp, F. *Int. J. Mass Spectom. Ion Processes* **1991**, *111*, 89.
(15) Beavis, R. C.; Chait, B. T. *Rapid Comm. Mass Spectrom.* **1989**, *3*, 432.
(16) Tanaka, K.; Hiroaki, W.; Ido, Y.; Akita, S.; Yoshida, Y.; Yoshida, T. *Rapid Commun. Mass Spectrom.* **1988**, *2*, 151.
(17) Dale, R.; Knochenmuss, R.; Zenobi, R *Rapid Commun. Mass Spectrom.* **1997**, *11*, 136.
(18) Kraft, P.; Alimpiev, S.; Dratz, E.; Sunner, J. *J. Am. Soc. Mass Spectrom.* **1998**, *9*, 912.
(19) Schürenberg, M.; Dreisewerd, K.; Hillenkamp, F. *Anal. Chem.* **1999**, *71*, 221.
(20) Dietemann, P.; Edelmann, M. J.; Meisterhans, C.; Pfeiffer, C.; Zumbuhl, S.; Knochenmuss, R.; Zenobi, R. *Helvetica Chim. Acta* **2000**, *83*, 1766.
(21) Handschuh, M.; Nettesheim, S.; Zenobi, R. *Appl. Surf. Sci.* **1999**, *137*, 125.
(22) Wei, J.; Buriak, J. M.; Siuzdak, G. *Nature* **1999**, *399*, 243.
(23) Berkenkamp, S.; Menzel, C.; Karas. M.; Hillenkamp, F. *Rapid Commun. Mass Spectrom.* **1997**, *11*, 1399.
(24) Dreisewerd, K.; Berkenkamp, S.; Leisner, A.; Rohlfing, A.; Menzel, C. *Int. J. Mass Spectrom.* **2003**, in press.
(25) Budnik, B. A.; Jensen, K. B.; Jorgenson, T. J. D.; Haase, A.; Zubarev, R. A. *Rapid Commun. Mass Spectrom.* **2000**, *14*, 578.
(26) Lippa, T.; Taranenko, N. I.; Prasad, C. R.; Doroshenko, V. M. *Eur. J. Mass Spectrom.* **2002**, *8*, 263.
(27) Overberg, A.; Karas, M.; Hillenkamp, F. *Rapid Commun. Mass Spectrom.* **1991**, *5*, 128.
(28) Menzel, C.; Berkenkamp, S.; Hillenkamp, F. *Rapid Commun. Mass Spectrom.* **1999**, *13*, 26.
(29) Cramer, R.; Haglund, R. F.; Hillenkamp, F. *Int. J. Mass Spectrom. Ion Processes* **1997**, *169/170*, 51.
(30) Ermer, D. R.; Baltz-Knorr, M.; Haglund, R. F. *J. Mass Spectrom.* **2001**, *36*, 538.
(31) aus der Wiesche, S.; Rembe, C.; Hofer, E. P. *Heat Mass Transfer* **1999**, *35*, 25.
(32) Miotello, A.; Kelly, R. *Appl. Phys. Lett.* **1995**, *67*, 3535.
(33) Venugopalan, V.; Nishioka, N. S.; Mikic, B. B. *Biophys. J.* **1996**, *70*, 2981.
(34) Venugopalan, V.; Vogel. A. *Chem. Rev.*, this issue.
(35) Lindner, B.; Seydel, U. *Anal. Chem.* **1985**, *57*, 895.
(36) Garrison, B. J.; Srinivasan, R. *Appl. Phys. Lett.* **1984**, *44*, 849.
(37) Laiko, V. V.; Baldwin, M. A.; Burlingame, A. L. *Anal. Chem.* **2000**, *72*, 652.
(38) Karas, M.; Bachmann, D.; Hillenkamp, F. *Anal. Chem.* **1985**, *57*, 2935.
(39) Horneffer, V.; Dreisewerd, K.; Luedemann, H.-C.; Hillenkamp, F.; Laege, M.; Strupat, K. *Int. J. Mass Spectrom.* **1999**, *185/186/187*, 859.
(40) Chen, X.; Caroll, J. A.; Beavis, R. C. *J. Am. Soc. Mass Spectrom.* **1998**, *9*, 885.
(41) Hillenkamp, F.; Karas, M.; Holtkamp, D.; Klüsener, P. *Int. J. Mass Spectrom. Ion Process.* **1986**, *69*, 265.
(42) Allwood, D. A.; Dreyfus, R. W.; Perera, I. K. *Rapid Commun. Mass Spectrom.* **1996**, *10*, 1575.
(43) Puretzky, A. A.; Geohegan, D. B. *Appl. Phys. Lett.* **1998**, *129*, 248.
(44) Allwood, D. A.; Dreyfus, R. W.; Perera, I. K.; Dyer, P. E. *Appl. Surface Sci.* **1997**, *110*, 154.
(45) Beavis, R. C.; Chait, B. T. *Rapid Commun. Mass Spectrom.* **1989**, *3*, 233.
(46) Wu, K. J.; Steding, A.; Becker, C. H. *Rapid Commun. Mass Spectrom.* **1993**, *7*, 142.
(47) Dreisewerd, K.; Spottke, B. University of Münster, 2001, unpublished data.
(48) Cornett, D. S.; Duncan, M. A.; Amster I. J. *Org. Mass Spectrom.* **1992**, *27*, 831.
(49) Cornett, D. S.; Duncan, M. A.; Amster I. J.; *Anal. Chem.* **1993**, *65*, 2608.
(50) Tang, K.; Allman S. L.; Jones R. B.; Chen C. H. *Org. Mass Spectrom.* **1992**, *27*, 1389.
(51) Smith, C. J.; Chang, S. Y.; Yeung, E. S. *J. Mass Spectrom.* **1995**, *30*, 1765.
(52) Hillenkamp, F.; Schulz, T.; Schuerenberg, M.; Dreisewerd, K. *Proceedings 45th ASMS Conference on Mass Spectrometry and Allied Topics*; Palm Springs, CA, June 1−5, 1997, p 1096.
(53) Demirev, P; Westman, A.; Rimann, C. T.; Hakansson, P.; Barofsky, D.; Sundqvist, B. U. R.; Chen, Y. D.; Seibt, W.; Siegbahn, K. *Rapid Commun. Mass Spectrom.* **1992**, *6*, 187.
(54) Yau, P. Y.; Chan, T.-W. D.; Gullis, P. G.; Colburn, A. W.; Derrick, P. J. *Chem. Phys. Lett.* **1993**, *202*, 93.
(55) Ingendoh, A.; Karas, M.; Hillenkamp, F.; Giessmann, U. *Int. J. Mass Spectrom. Ion Process.* **1994**, *131*, 345.
(56) Dreisewerd, K.; Schürenberg, M.; Karas, M.; Hillenkamp, F. *Int. J. Mass Spectrom. Ion Process.* **1994**, *141*, 127.
(57) Zhigilei, L. V.; Garrision, B. J.; *J. Appl. Phys.* **2000**, *88*, 1281.
(58) Wang, B. H.; Dreisewerd, K.; Bahr, U.; Karas, M.; Hillenkamp, F. *J. Am. Soc. Mass Spectrom.* **1993**, *4*, 393.
(59) Knochenmuss, R.; Dubois, F.; Dale, M. J.; Zenobi, R. *Rapid Commun. Mass Spectrom.* **1996**, *10*, 871.
(60) Knochenmuss, R.; Karbach, V.; Wiesli, U.; Breuker, K.; Zenobi, R. *Rapid Commun. Mass Spectrom.* **1998**, *12*, 529.
(61) Zhigilei, L. V.; Garrison, B. J. *Appl. Phys. Lett.* **1997**, *71*, 551.
(62) Zhigilei, L. V.; Garrison, B. J. *Appl. Phys. A* **1999**, *69*, Suppl. Dec., S75−S80.
(63) Zhigilei, L. V.; Garrison, B. J. *Rapid Commun. Mass Spectrom.* **1998**, *12*, 1273.
(64) Yangling, Y. G.; Zhigilei, L. V.; Garrison, B. J.; Koubenakis, A.; Labrakis, J.; Georgiou, S. *Appl. Phys. Lett.* **2001**, *78*, 1631.
(65) Ens, W.; Mao, Y.; Mayer, K. G.; Standing, K. G. *Rapid Commun. Mass Spectrom.* **1991**, *5*, 117.
(66) Westmacott, G.; Ens, W.; Hillenkamp, F.; Dreisewerd, K.; Schürenberg, M. *Int. J. Mass Spectrom.* **2002**, *221*, 67.
(67) Quist, A. P.; Huth-Fehre, T.; Sundqvist, B. U. R. *Rapid Commun. Mass Spectrom.* **1994**, *8*, 149.
(68) Spengler, B.; Bahr. U.; Karas, M.; Hillenkamp, F. *Anal. Instrum.* **1988**, *17*, 133.
(69) Huth-Fehre, C.; Becker, C. H. *Rapid Commun. Mass Spectrom.* **1991**, *5*, 378.
(70) Quist, P.; Huth-Fehre, T.; Sundqvist, B. U. R.; *Rapid Commun. Mass Spectrom.* **1994**, *8*, 149.
(71) Riahi, K.; Bolbach, G.; Brunot, A.; Breton, F.; Spiro, M.; Blais, J.-C. *Rapid Commun. Mass Spectrom.* **1994**, *8*, 242.
(72) Mowry; C. D.; Johnston, M. V. *Rapid Commun. Mass Spectrom.* **1993**, *7*, 569.
(73) Mowry, C. D.; Johnston, M. V. *J. Phys. Chem.* **1994**, *98*, 1904.
(74) Dreisewerd, K.; Schürenberg, M.; Karas, M.; Hillenkamp, F. *Int. J. Mass Spectrom. Ion Process.* **1996**, *154*, 171.
(75) Schürenberg, M.; Dreisewerd, K., Kamanabrou, S.; Hillenkamp, F. *Int. J. Mass Spectrom. Ion Process.* **1998**, *172*, 89.
(76) Vertes,A.; Gijbels, R.; Levine, R. D. *Rapid Commun. Mass Spectrom.* **1990**, *4*, 228.
(77) Brown, R. S.; Lennon, J. J. *Anal. Chem.* **1995**, *67*, 3990.
(78) Kaufmann, R.; Spengler, B,; Lützenkirchen, F. *Rapid Commun. Mass Spectrom.* **1993**, *7*, 902.
(79) Spengler, B. J. *Mass Spectrom.* **1997**, *32*, 1019.
(80) Benscura, A.; Navale, V.; Sadeghi, M.; Vertes, A. *Rapid Commun. Mass Spectrom.* **1997**, *11*, 679.
(81) Dlott, D. D. *J. Opt. Soc.* **1990**, *89*, *830*.
(82) Johnson, R. E. *Int. J. Mass Spectom. Ion Process.* **1994**, *139*, 25.
(83) Esenaliev, R. O.; Oraevsky, A. A.; Lethokov, V. S.; Karabutov, A. A.; Malinsky, T. V. *Lasers Surg. Med.* **1993**, *13*, 470.
(84) Menzel, C.; Dreisewerd, K.; Berkenkamp, S.; Hillenkamp, F. *Int. J. Mass Spectrom.* **2001**, *207*, 73.
(85) Menzel, C.; Dreisewerd, K.; Berkenkamp, S.; Hillenkamp, F. *J. Am. Soc. Mass Spectrom.* **2002**, *13*, 975.
(86) Zhigilei, L. V.; Kodali, P. B. S.; Garrison, B. J. *Chem. Phys. Lett.* **1997**, *276*, 269.
(87) Zhigilei, L. V.; Kodali, P. B. S.; Garrison, B. J. *J. Phys. Chem. B* **1998**, *102*, 2845.
(88) Zhigilei, Z. V.; Yingling, Y. G.; Itina, T. E.; Schoolcraft, T. A.; Garrison, B. J. *Int. J. Mass Spectrom.*, in press.
(89) Zhigilei, L. V.; Kodali, P. B. S.; Garrison, B. J. *J. Phys. Chem. B* **1997**, *101*, 2028.
(90) Schäfer, C.; Urbassek, H. M.; Zhigilei, L. V.; Garrison, B. J. *Comp. Mater. Sci.* **2002**, *24*, 421.
(91) Y. G. Yingling, L. V. Zhigilei, B. J. Garrison, A. Koubenakis, J. Labrakis, S. Georgiou *Appl. Phys. Lett.* **2001**, *78*, 1631.
(92) Itina, T. E.; Zhigilei, L. V.; Garrison, B. J. *J. Phys. Chem. B* **2002**, *106*, 303.
(93) Zeifman, M. I.; Garrison, B. J.; Zhigilei, L. V. *Appl. Surf. Sci.* **2002**, *197/198*, 271.
(94) Zeifman, M. I.; Garrison, B. J.; Zhigilei, L. V. *J. Appl. Phys.* **2002**, *92*, 2181.
(95) Antonov, V. S.; Lethokov, V. S.; Matveyets, Y. A.; Shibanov, A. N. *Laser Chem.* **1982**, *1*, 37.
(96) Chekalin, S. V.; Golovlev, V. V.; Kozlov, A. A.; Matveyets, Y. A.; Yartsev, A. P.; Lethokov, V. S. *Phys. Chem.* **1988**, 6855.
(97) Knochenmuss, R.; Vertes, A. *J. Phys. Chem. B* **2000**, *104*, 5406.
(98) Knochenmuss, R. *J. Mass Spectrom.* **2002**, *37*, 867.
(99) Ehring, H.; Sundqvist, B. U. R. *J. Mass Spectrom.* **1995**, *30*, 1303.
(100) Lüdemann, H. C.; Anderson, R.; Hillenkamp, F. *Rapid Commun. Mass Spectrom.* **2002**, *16*, 1287.
(101) Hillenkamp, F.; Karas, M.; Bahr, U.; Ingendoh, A. In *Ion Formation from Organic Solids (IFOS V)*; Hedin, A.; Sundqvist, B. U. R.; Benninghoven, A., Eds., Wiley & Sons Inc., Chichester, 1990; p 111.
(102) Brannon, J.; Lankard, J. R.; Baise, A. I.; Burns, F.; Kaufman, J. *J. Appl. Phys.* **1985**, *58*, 2036.
(103) Kelly, R.; Miotello, A. *Phys. Rev. E* **1999**, *60*, 2616.

(104) aus der Wiesche, S.; Rembe, C.; Hofer, E. P. *Heat Mass Transfer* **1999**, *35*, 23.
(105) Debendetti, P. *Metastable Liquids: Concepts and Principles*; Princeton University Press: Princeton, NJ, 1996.
(106) Fournier, I.; Tabet, J. C.; Bolbach, G. *Int. J. Mass Spectrom.* **2002**, *219*, 515.
(107) von Allmen, M. *Laser-Beam Interactions with Materials*; Springer: Berlin, 1987.
(108) Williams, B. W.; Irsa, A. P.; Zmora, H.; Beuhler, R. J. *J. Phys. Chem.* **1983**, *87*, 2185.
(109) Knochenmuss, R.; Stortelder, A.; Breuker, K.; Zenobi, R. *J. Mass Spectrom.* **2000**, *35*, 1237.
(110) Seiler, T.; McDonnel, P. J. *Surv. Ophthalmol.* **1995**, *40*, 89.
(111) Garrison, B. J.; Srinivasan, R. F. *Appl. Phys. Lett.* **1985**, *57*, 909.
(112) Vertes, A.; Dreyfus, R. W.; Platt, D. E. *IBM J. Res. Develop.* **1994**, *38*, 3.
(113) Vertes, A.; Iriny, G.; Gijbels, R. *Anal. Chem.* **1993**, *65*, 2389.
(114) Linder, B.; Seydel, U. *Anal. Chem.* **1985**, *57*, 895.
(115) Perez, J.; Petzold, C. J.; Watkins, M. A.; Vaughn, W. E.; Kenttamaa, H. I. *J. Am. Soc. Mass Spectrom.* **1999**, *10*, 1105.
(116) Galicia, M. C.; Vertes, A.; Callahan, J. H. *Anal. Chem.* **2002**, *74*, 1891.
(117) Schürenberg, M.; Schulz, T.; Dreisewerd, K.; Hillenkamp, F. *Rapid Commun. Mass Spectrom.* **1996**, *10*, 1873.
(118) Linder, B. *Int. J. Mass Spectrom. Ion Process.* **1991**, *103*, 203.
(119) Ehring, H.; Costa, C.; Demirev, P. A.; Sundqvist, B. U. R. *Rapid Commun. Mass Spectrom.* **1996**, *10*, 821.
(120) Golovlev, V. V.; Allman, S. L.; Garrett, W. R.; Taranenko, N. I.; Chen, C. H. *Int. J. Mass Spectrom. Ion Process.* **1997**, *169/170*, 69.
(121) Lindner, B.; Seydel, U. *Anal. Chem.* **1985**, *57*, 895.
(122) Itina, T. E.; Zhigilei, L. V.; Garrison, B. J. *Nucl. Instrum. Meth. B.* **2001**, *180*, 238.
(123) Krutchinsky, A. N.; Chait, B. N. *J. Am. Soc. Mass Spectrom.* **2002**, *13*, 129.
(124) Bahr, U.; Röhling U.; Lautz, C.; Strupat, K.; Schürenberg, M.; Hillenkamp, F. *Int. J. Mass Spectrom. Ion Process.* **1996**, *153*, 9.
(125) Ford, T. A.; Falk, M. *Can. J. Chem.* **1968**, *46*, 3579.
(126) Karas, M.; Glückmann, M.; Schäfer, J. *J. Mass Spectrom.* **2000**, *35*, 1.
(127) Karbach V.; Knochenmuss, R. *Rapid Commun. Mass Spectrom.* **1998**, *12*, 968.
(128) Lin, Q.; Kochenmuss, R. *Rapid Commun. Mass Spectrom.* **2001**, *15*, 1422.
(129) Land, C. M.; Kinsel, G. R. *J. Am. Soc. Mass Spectrom.* **2001**, *12*, 726.
(130) Fournier, I.; Brunot, A.; Tabet, J. C.; Bolbach, G. *Int. J. Mass Spectrom.* **2002**, *213*, 203.
(131) Jespersen, S.; Niessen, W. M. A.; Tjaden, U. R.; van der Greef, J.; Litborn, E.; Lindberg, U.; Roeraade, J. *Rapid Commun. Mass Spectrom.* **1994**, *8*, 581.
(132) Keller, B. O.; Li, L. *J. Am. Soc. Mass Spectrom.* **2001**, *12*, 1055.
(133) Vorm, O.; Roepstorff, P.; Mann, M. *Anal. Chem.* **1994**, *66*, 3281.
(134) Haisa, M.; Kashino, S.; Hanada, S.-I.; Tanaka, K.; Okazaki, S.; Shibagaki, M. *Acta Crystallogr. B* **1982**, *38*, 1480.
(135) Spengler, B.; Hubert, M. *J. Am. Soc. Mass Spectrom.* **2002**, *13*, 735.
(136) Nordhoff, E.; Ingendoh, A.; Cramer, R.; Overberg, A.; Stahl, B.; Karas, M.; Hillenkamp, F.; Crain, P. F. *Rapid Commun. Mass Spectrom.* **1992**, *6*, 771.
(137) Liao, P.-C.; Allison, J. *J. Mass Spectrom.* **1995**, *30*, 408.
(138) Bahuk, A.; Gluch, K.; Michalak, L. *Rapid Commun. Mass Spectrom.* **2001**, *15*, 2383.
(139) Medina, M.; Huth-Fehre, T.; Westman, A.; Sundqvist, B. U. R. *Org. Mass Spectrom.* **1994**, *29*, 207.
(140) Duncan, M. W.; Matanovic, G.; Cerapoljak, A. *Rapid Commun. Mass Spectrom.* **1993**, *7*, 1090.
(141) Nelson, R. W.; Mc Lean, M. A.; Hutchens, T. W. *Anal. Chem.* **1994**, *66*, 1408.
(142) Jimenez, C. R.; Li, K. W.; Dreisewerd, K.; Mansvelder, H. D.; Brussaard, A. B.; Reinhold, B. B.; Van der Schors, R. C.; Karas, M.; Hillenkamp, F.; Burbach, J. P. H.; Costello, C. E.; Geraerts, W. P. M. *Proc. Natl. Acad. Sci. U.S.A.* **1997**, *94*, 9481.
(143) Kampmeier, J.; Dreisewerd, K.; Schürenberg, M.; Strupat, K. *Int. J. Mass Spectom. Ion Process.* **1997**, *169/170*, 31.
(144) Kim, S. H.; Shin, C. M.; Yoo, J. S. *Rapid Commun. Mass Spectrom.* **1998**, *12*, 701.
(145) Sadeghi, M.; Vertes, A. *Appl. Surf. Sci.* **1998**, *127*−*129*, 226.
(146) Xiang, F.; Beavis, R. C. *Rapid Commun. Mass Spectrom.* **1994**, *8*, 199.
(147) Onnerfjord, P.; Ekstrom, S.; Bergquist, H.; Nilsson, J.; Laurell, T.; Barko-Varga, G. *Rapid Commun. Mass Spectrom.* **1999**, *13*, 315.
(148) Doktycz, S. J.; Savickas, P. J.; Krueger, D. A. *Rapid Commun. Mass Spectrom.* **1991**, *5*, 145.
(149) Hensel, R. R.; King, R. G.; Owens, K. G. *Rapid Commun. Mass Spectrom.* **1997**, *11*, 1785.
(150) Dai, Y.; Whittal, R. M..; Li, L. *Anal. Chem.* **1996**, *68*, 2494.
(151) Horneffer, V.; Forsmann, A.; Strupat, K.; Hillenkamp, F.; Kubitscheck, U. *Anal. Chem.* **2001**, *73*, 1016.
(152) Chan, D. T. W.; Colburn, A. W.; Derrick, P. J. *Org. Mass Spectrom.* **1992**, *27*, 188.
(153) Westman, A.; Huth-Fehre, T.; Demirev, P.; Sundqvist, B. U. R. *J. Mass Spectrom.* **1995**, *30*, 206.
(154) Gusev, A. I.; Wilkinson, W. R.; Proctor, A.; Hercules, D. M. *Anal. Chem.* **1995**, *67*, 1034.
(155) Horneffer, V.; Reichelt, R.; Strupat, K. *Int. J. Mass Spectrom.* **2003**, in press.
(156) Glückmann, M.; Pfenninger, A.; Krüger, R.; Thierolf, M.; Karas, M.; Horneffer, V.; Hillenkamp, F.; Strupat, K. *Int. J. Mass Spectrom.* **2001**, *210/211*, 121.
(157) Horneffer, V.; Glückmann, M.; Krüger, R.; Pfenninger, A.; Thierolf, M.; Fournier, I.; Kubitscheck, U.; Hillenkamp, F.; Karas, M.; Strupat, K., manuscript in preparation.
(158) Beavis, R. C.; Bridson, J. N. *J. Phys. D.* **1993**, *26*, 442.
(159) Garden, R. W.; Sweedler, J. V. *Anal. Chem.* **2000**, *72*, 30.
(160) Spengler, B.; Huber, M. *J. Am. Soc. Mass Spectrom.* **2002**, *13*, 735.
(161) Krüger, R.; Pfenninger, A.; Fournier, I.; Glückmann, M.; Karas, M. *Anal. Chem.* **2001**, *73*, 5812.
(162) Brown, R. S.; Durrant, E. E. *Proceedings of the 50th ASMS Conference on Mass Spectrometry and Allied Topics*, Orlando, FL, June 2−6, 2002, code MPL 366.
(163) Skelton, R.; Dubois F.; Zenobi, R. *Anal. Chem.* **2000**, *72*, 1707.
(164) Timpin, S.; Rouhanipour, A.; Az, R.; Rader, H. J.; Mullen, K. *Rapid Commun. Mass Spectrom.* **2001**, *15*, 1364.
(165) Wang, M. Z.; Fitzgerald, M. C. *Anal. Chem.* **2001**, *73*, 625.
(166) Kussman, M. E.; Nordhoff, E.; Rahbek-Nielsen, H.; Haebel, S.; Rossel-Larsen, M.; Jakobsen, L.; Gobom, J.; Mirgorodskaya, E.; Kroll-Kristensen, A.; Palm, L.; Roepstorff, P. *J. Mass Spectrom.* **1997**, *32*, 593.
(167) Onnerfjord, P.; Ekstrom, S.; Bergquist, J.; Nilsson, J.; Laurell, T.; Marko-Varga, G. *Rapid Commun. Mass Spectrom.* **1999**, *13*, 315.
(168) Miliotis, T.; Kjellstrom, S.; Nilsson, J.; Laurell, T.; Edholm, L. E.; Marko-Varga, G. *Rapid Commun. Mass Spectrom.* **2002**, *16*, 117.
(169) Haddleton, D. M.; Waterson, C.; Derrick, P. J. *Eur. Mass Spectrom.* **1998**, *4*, 203.
(170) Axelsson, J.; Hoberg, A. M.; Waterson, C.; Myatt, P.; Shield, G. L.; Varney, J.; Haddleton, D. M.; Derrick, P. J. *Rapid Commun. Mass Spectrom.* **1997**, *11*, 209.
(171) Preisler, J.; Foret, F.; Karger, B. L. *Anal. Chem.* **1998**, *70*, 5278.
(172) Preisler, J.; Hu, P.; Rejtar, T.; Karger, B. L. *Anal. Chem.* **2000**, *72*, 4785.
(173) Cohen, S. L.; Chait, B. T. *Anal. Chem.* **1996**, *68*, 31.
(174) Bornsen, K. O.; Gass, M. A. S.; Bruin, G. J. M.; Von Adrichem, J. H. M.; Biro, M. C.; Kresbach, G. M.; Ehrat, M. *Rapid Commun. Mass Spectrom.* **1997**, *11*, 603.
(175) Huff, T.; Muller, C. S. G.; Hannappel, E. *FEBS Lett.* **1997**, *414*, 39.
(176) Nilsson, C. L.; Brodin, E. J. *Chromatogr. A* **1998**, *800*, 21.
(177) Stahl, B.; Linos, A.; Karas, M.; Hillenkamp, F.; Steup, M. *Anal. Biochem.* **1997**, *246*, 195.
(178) Dreisewerd, K.; Kingston, R.; Geraerts, W. P. M.; Li, K. W. *Int. J. Mass Spectrom. Ion Process.* **1997**, *169*, 291.
(179) Jimenez, C. R.; van Veelen, P. A.; Li, K. W.; Wildering, W. C.; Geraerts, W. P. M.; Tjaden, U. R.; Van der Greef, J. *J. Neurochem.* **1994**, *62*, 404.
(180) Garden, R. W.; Moroz, L. L.; Moroz, T. P.; Shippy, S. A.; Sweedler, J. V. *J. Mass Spectrom.* **1996**, *31*, 1126.
(181) Jimenez, C. R.; Li, K. W.; Dreisewerd, K.; Spijker, S.; Kingston, R.; Bateman, R. H.; Burlingame, A. L.; Smit, A. B.; van Minnen, J.; Geraerts, W. P. M. *Biochem.* **1998**, *37*, 2070.
(182) Fenselau, C.; Demirev, P. A. *Mass Spectrom. Rev.* **2001**, *20*, 157.
(183) Welham, K. J.; Domin, M. A.; Scannell, D. E.; Cohen, E.; Ashton, D. S. *Rapid Commun. Mass Spectrom.* **1998**, *12*, 176.
(184) Wang, Z. P.; Rosson, L.; Li, L.; Roser, D. C.; Long, S. R. *Rapid Commun. Mass Spectrom.* **1998**, *12*, 456.
(185) Amiri-Eliasi, B. J.; Fenselau, C. *Anal. Chem.* **2001**, *73*, 5228.
(186) Caprioli, R. M.; Farmer, T. B.; Gile, J. *Anal. Chem.* **1997**, *69*, 4751.
(187) Todd, P. J.; Schaaff, T. G.; Chaurand, P.; Caprioli, R. M. *J. Mass Spectrom.* **2001**, *36*, 355.
(188) Chaurand, P.; DaGue, B. B.; Pearsall, R. S.; Threadgill, D. W.; Caprioli, R. M. *Proteomics* **2001**, *1*, 1320.
(189) Chaurand, P.; Stockli, M.; Caprioli, R. M. *Anal. Chem.* **1999**, *71*, 5263.
(190) Loo, R. R. O.; Stevenson, T. I.; Mitchell, C.; Loo, J. A.; Andrews, P. C. *Anal. Chem.* **1996**, *68*, 1910.
(191) Guittard, J.; Hronowski, X. P. L.; Costello, C. E. *Rapid Commun. Mass Spectrom.* **1999**, *13*, 1838.
(192) Gusev, A. I.; Proctor, A.; Rabinovich, Y. I.; Hercules, D. M. *Anal. Chem.* **1995**, *67*, 1805.
(193) Gusev, A. I. *Fresenius. J. Anal. Chem.* **2000**, *366*, 691.
(194) Castoro, J. A.; Wilkins, C. L. *Anal. Chem.* **1993**, *65*, 2621.

(195) Gusev, A. I.; Wilkinson, W. R.; Proctor, A.; Hercules, D. M. *Anal. Chem.* **1995**, *67*, 1034.
(196) Hung, K. C.; Ding, H.; Guo, B. C. *Anal. Chem.* **1999**, *71*, 518.
(197) Yuan, X. L.; Desiderio, D. M. *J. Mass Spectrom.* **2002**, *37*, 512.
(198) Zaluzec, E. J.; Gage, D. A.; Allison, J.; Watson, J. T.; *J. Am. Soc. Mass Spectrom.* **1994**, *5*, 230.
(199) Walker, A. K.; Wu, Y. L.; Timmons, R. B.; Kinsel, G. R.; Nelson, K. D. *Anal. Chem.* **1999**, *71*, 268.
(200) Hung, K. C.; Rashidzadeh, H.; Wang, Y.; Guo, B. C. *Anal. Chem.* **1998**, *70*, 3088.
(201) Schürenberg, M.; Luebbert, C.; Eickhoff, H.; Kalkum, M.; Lehrach, H.; Nordhoff, E. *Anal. Chem.* **2000**, *72*, 3436.
(202) Little, D. P.; Cornish, T. J.; O'Donnell, M. J.; Braun, A.; Cotter, R. J., Köster, H. *Anal. Chem.* **1997**, *69*, 4540.
(203) Buetow, K. H.; Edmonson, M.; McDonald, R.; Clifford, R.; Yip, P.; Kelley, J.; Little, D. P.; Strausberg, R.; Köster H.; Cantor, C. R.; Braun, A. *Proc. Natl. Acad. Soc. Sci. U.S.A.* **2001**, *98*, 581.
(204) Westman, A.; Demirev, P.; Huth-Fehre, T.; Bielawski, J.; Sundqvist, B. U. R. *Int. J. Mass Spectrom. Ion Process.* **1994**, *130*, 107.
(205) Fournier I.; Beavis, R. C.; Blais, J. C.; Tabet, J. C.; Bolbach, G. *Int. J. Mass Spectrom. Ion Process.* **1997**, *169/170*, 19.
(206) Fournier, I.; Strupat, K.; Horneffer, V., private communication, 2001.
(207) *Lambda Highlights* **1990**, *25*, 7.
(208) Dyer, P. E.; Jenkins, S. D.; Sidhu, J. *Appl. Phys. Lett.* **1986**, *49*, 453.
(209) Dyer, P. E.; Jenkins, S. D.; Sidhu, J. *Appl. Phys. Lett.* **1987**, *52*, 1880.
(210) Juhasz, P.; Vestal, M. L.; Martin, S. A. *J. Am. Soc. Mass Spectrom.* **1997**, *8*, 209.
(211) Glückmann, M.; Karas, M. *J. Mass Spectrom.* **1999**, *34*, 467.
(212) Beavis, R. C.; Chait, B. T. *Chem. Phys. Lett.* **1991**, *181*, 479.
(213) Zhang, W.; Chait, B. T. *Int. J. Mass Spectrom. Ion Process.* **1997**, *160*, 259.
(214) Pan, Y.; Cotter, R. J. *Org. Mass Spectrom.* **1992**, *27*, 3.
(215) Huth-Fehre, T.; Becker, C. H. *Rapid Commun. Mass Spectrom.* **1991**, *5*, 378.
(216) Zhou, J.; Ens, W.; Standing, K. G.; Verentchikov, A. *Rapid Commun. Mass Spectrom.* **1992**, *6*, 671.
(217) Spengler, B.; Bökelmann, V. *Nucl. Instrum. Meth. Phys. Res. B* **1993**, *82*, 379.
(218) Bökelmann, V.; Spengler, B.; Kaufmann, R. *Eur. Mass Spectrom.* **1995**, *1*, 81.
(219) Kinsel, G. R.; Edmondson, R. D.; Russell, D. H. *J. Mass Spectrom.* **1997**, *32*, 714.
(220) Puretzky, A. A.; Geohegan, D. B.; Hurst, G. B.; Buchanan, M. V.; Luk'yanchuk, B. S. *Phys. Rev. Lett.* **1999**, *83*, 444.
(221) Kinsel, G. R.; Gimon-Kinsel, M. E.; Gillig, K. J.; Russell, D. H. *J. Mass Spectrom.* **1999**, *34*, 684.
(222) Chan, T. W. D.; Thomas, I.; Colburn, A. W.; Derrick, P. J. *Chem. Phys. Lett.* **1994**, *226*, 579.
(223) Ermer, E. R.; Baltz-Knorr, M.; Haglund, R. F. *J. Mass Spectrom.* **2001**, *36*, 538.
(224) Berkenkamp, S.; Menzel, C.; Hillenkamp, F.; Dreisewerd, K. *J. Am. Soc. Mass Spectrom.* **2002**, *13*, 209.
(225) van der Peyl, G. J. Q.; van der Zande, W. J.; Kistemaker, P. G. *Int. J. Mass Spectrom. Ion Processes* **1984**, *62*, 51.
(226) Engelke, F.; Hahn, J. H.; Henke, W.; Zare, R. N. *Anal. Chem.* **1987**, *59*, 909.
(227) Voumard, P.; Zenobi, R.; Zhan, Q *Surf. Sci.* **1994**, *307*, 360.
(228) Elam, J. W.; Levy, D. H. *J. Phys. Chem. B* **1998**, *102*, 8113.
(229) Tabet, J.-C.; Cotter, R. J. *Int. J. Mass Spectrom. Ion Processes* **1983**, *54*, 151.
(230) Buck, M.; Hess, P. *J. Electron Spectrosc. Relat. Phenom.* **1987**, *45*, 237.
(231) Danielzik, B.; Fabricius, N.; Röwekamp, M.; van der Linde, D. *Appl. Phys. Lett.* **1986**, *48*, 212.
(232) Yang, M.; Reilly, J. P. *J. Phys. Chem.* **1990**, *94*, 6299.
(233) Spengler, B.; Cotter, R. J. *Anal. Chem.* **1990**, *62*, 793.
(234) Georgiou, S.; Koubenakis, A.; Labrakis, J.; Lassithiotaki, M. *Appl. Surf. Sci.* **1998**, *127−129*, 122.
(235) Grivas, C.; Nino, H.; Yabe, A. *Appl. Phys. A (Suppl.)* **1999**, *69*, S159.
(236) Franzen, J. *Int. J. Mass Spectrom. Ion Processes* **1997**, *164*, 19.
(237) Johnson, R. E.; LeBeyec, Y. *Int. J. Mass Spectrom.* **1998**, *177*, 111.
(238) Wu, X. W.; Sadeghi, M.; Vertes, A. *J. Phys. Chem. B* **1998**, *102*, 4770.
(239) Puretzky, A. A.; Geohegan, D. B. *Appl. Surf. Sci.* **1998**, *127−129*, 248.
(240) Castoro, J. A.; Wilkins, C. L. *Anal. Chem.* **1993**, *65*, 2621.
(241) Heise, T. W.; Yeung, E. S. *Anal. Chem.* **1994**, *66*, 355.
(242) Comsa, G.; David, R. *Surf. Sci. Rep.* **1985**, *5*, 145.
(243) Levis, R. J. *Annu. Rev. Phys. Chem.* **1994**, *45*, 483.
(244) Karas, M.; Dreisewerd, K.; Schürenberg, M.;Wang, B. H.; Hillenkamp, F. In: *AIP Conf. Proc.* **1995**, *329*, 53.
(245) Chang, M. C.; Petrich, D. B.; McDonald, G. R.; Fleming, J. J. Am. Chem. Soc. **1983**, *105*, 3819.
(246) Petrich, J. W.; Chang, M. C.; McDonald, D. B.; Fleming, G. R. *J. Am. Chem. Soc.* **1983**, *105*, 3824.
(247) Chen, K. R.; King, T. C.; Hes, J. H.; Neboeuf, J. N.; Geohegan, D. B.; Wood, R. F.; Puretzky, A. A.; Doanto, J. M. *Phys. Rev. B.* **1999**, *60*, 8373.
(248) Sibold, D.; Urbassek, H. M. *J. Appl. Phys.* **1993**, *73*, 8544.
(249) Kelly, R. *J. Chem. Phys.* **1990**, *92*, 5047.
(250) Kelly, R.; Dreyfus, R. W., *Nucl. Instrum. Meth. Phys. Res. B* **1988**, *32*, 241.
(251) Kelly R.; Miotello, A. *Nucl. Instrum. Meth. Phys. Res. B* **1997**, *122*, 374.
(252) Noorbatcha, I.; Lucchese, R. R.; Zeiri, Y. *Phys. Rev. B* **1987**, *36*, 4978.
(253) Cowin, J. P.; Auerbach, D. J.; Becker, C.; Wharton, L. *Surf. Sci.* **1978**, *78*, 545.
(254) Miller, D. R. in Soles, G. (ed.) *Atomic and Molecular Beam Methods*, Oxford University Press, Oxford, 1988, p 14.
(255) Chen, K. R.; Neboeuf, J. N.; Wood, R. F.; Geohegan, D. B.; Donato, J. M.; Liu, C. L.; Puretzky, A. A. *Phys. Rev. Lett.* **1995**, *75*, 4706.
(256) Kools, J. C. S.; Baller, T. S.; De Zwart, S. T.; Dieleman, J. *J. Appl. Phys.* **1992**, *71*, 4547.
(257) Itina, T. E.; Katassonov, A. A.; Marine, W.; Autric, M.*J. Appl. Phys.* **1998**, *83*, 6050.
(258) Puretzky, A. A.; Geohegan, D. B. *Chem. Phys. Lett.*, **1998**, *286*, 425.
(259) O'Connor, P. B.; Costello, C. E. *Rapid Commun. Mass Spectrom.* **2001**, *15*, 1862.
(260) Krutchinsky, A. N.; Loboda, A. V.; Spicer, V. L.; Dworschak, R; Ens, W.; Standing, K. G. *Rapid Commun. Mass Spectrom.* **1998**, *12*, 508.
(261) Stevenson, E.; Breuker, K.; Zenobi, R. *J. Mass Spectrom.* **2000**, *35*, 1035.
(262) Stahl, B.; Steup, M.; Karas, M.; Hillenkamp, F. *Anal. Chem.* **1991**, *63*, 1463.
(263) Wu, K. J.; Odom, R. W. *Anal. Chem.* **1998**, *70*, 456A.
(264) Poehlein, S. K.; Dormady, S. J.; McMillin, D. R.; Regnier, F. E. *Rapid Commun. Mass Spectrom.* **1999**,*13*, 1349.
(265) Lüdemann, H.-C. Ph.D. thesis, University of Münster, 2001.

CR010375I